



A cytoskeleton-membrane interaction conserved in fast-spiking neurons controls movement, emotion, and memory

Di Ma, Chao Sun, Rahul Manne, Tianqi Guo, Christophe Bosc, Joshua Barry,
Thomas Magliery, Annie Andrieux, Houzhi Li, Chen Gu

► To cite this version:

Di Ma, Chao Sun, Rahul Manne, Tianqi Guo, Christophe Bosc, et al.. A cytoskeleton-membrane interaction conserved in fast-spiking neurons controls movement, emotion, and memory. *Molecular Psychiatry*, 2023, 28 (9), pp.3994-4010. 10.1038/s41380-023-02286-7 . inserm-04704145

HAL Id: inserm-04704145

<https://inserm.hal.science/inserm-04704145v1>

Submitted on 20 Sep 2024

HAL is a multi-disciplinary open access archive for the deposit and dissemination of scientific research documents, whether they are published or not. The documents may come from teaching and research institutions in France or abroad, or from public or private research centers.

L'archive ouverte pluridisciplinaire **HAL**, est destinée au dépôt et à la diffusion de documents scientifiques de niveau recherche, publiés ou non, émanant des établissements d'enseignement et de recherche français ou étrangers, des laboratoires publics ou privés.

A cytoskeleton-membrane interaction conserved in fast-spiking neurons controls movement, emotion, and memory

Di Ma^{1,2}, Chao Sun^{2,3}, Rahul Manne², Tianqi Guo⁴, Christophe Bosc⁵, Joshua Barry^{2,\$}, Thomas Magliery⁴,
Annie Andrieux⁵, Houzhi Li², and Chen Gu^{1,2,3*}

¹Ohio State Biochemistry Graduate Program

²Department of Biological Chemistry and Pharmacology

³MCDB graduate program

⁴Department of Chemistry and Biochemistry

The Ohio State University, Columbus, OH 43210, USA

⁵Univ. Grenoble Alpes, Inserm, U1216, CEA, Grenoble Institut Neurosciences, 38000 Grenoble, France.

^{\$}Current address: IDDRRC, Jane and Terry Semel Institute for Neuroscience and Human Behavior, David Geffen School of Medicine, University of California Los Angeles, Los Angeles, CA, USA.

^{*}To whom correspondence should be addressed:

Chen Gu, Ph.D., 182 Rightmire Hall, 1060 Carmack Road, The Ohio State University, Columbus, OH 43210. Phone: 614-292-0349; Fax: 614-292-5379; Email: gu.49@osu.edu

Abstract

The pathogenesis of schizophrenia is believed to involve combined dysfunctions of many proteins including microtubule-associated protein 6 (MAP6) and Kv3.1 voltage-gated K⁺ (Kv) channel, but their relationship and functions in behavioral regulation are often not known. Here we report that MAP6 stabilizes Kv3.1 channels in parvalbumin-positive (PV+) fast-spiking GABAergic interneurons, regulating behavior. MAP6^{-/-} and Kv3.1^{-/-} mice display similar hyperactivity and avoidance reduction. Their proteins colocalize in PV+ interneurons and MAP6 deletion markedly reduces Kv3.1 protein level. We further show that two microtubule-binding modules of MAP6 bind the Kv3.1 tetramerization domain with high affinity, maintaining the channel level in both neuronal soma and axons. MAP6 knockdown by AAV-shRNA in the amygdala or the hippocampus reduces avoidance or causes hyperactivity and recognition memory deficit, respectively, through elevating projection neuron activity. Finally, knocking down Kv3.1 or disrupting the MAP6-Kv3.1 binding in these brain regions causes avoidance reduction and hyperactivity, consistent with the effects of MAP6 knockdown. Thus, disrupting this conserved cytoskeleton-membrane interaction in fast-spiking neurons causes different degrees of functional vulnerability in various neural circuits.

Keywords: Microtubule-associated protein 6 (MAP6); KCNC1/Kv3.1; Parvalbumin-positive (PV+) GABAergic interneuron; Amygdala; Hippocampus; Hyperactivity; Risk avoidance; Recognition memory.

Introduction

Schizophrenia is a severe mental disorder that affects approximately 1% of the population and is characterized by a disintegration of cognitive and emotional processes that affect the individual's behaviors. The pathogenesis of schizophrenia remains poorly understood, but it clearly contains a genetic component. Genome-wide association analysis and exome meta-analysis have identified more than 100 risk genes for schizophrenia and related mental disorders¹⁻⁴. Dysfunction of many proteins has been implicated in its pathogenesis, but the functions of most of these proteins appear unrelated, such as microtubule-associated protein 6 (MAP6) and Kv3.1 voltage-gated K⁺ (Kv) channel⁵⁻¹¹. Therefore, a better understanding of their functional relationship and individual impact on behavior may help to uncover the core pathogenic mechanism and ultimately to develop new rationale therapies.

MAP6 expression deficits were found in humans with mental disorders including schizophrenia⁵⁻⁹. MAP6, initially called stable-tubule-only polypeptide, was identified and cloned due to its unique ability to confer remarkable cold stability onto microtubules (MTs)¹²⁻¹⁴. Subsequent studies showed that MAP6 is a vertebrate-specific and multi-functional protein containing different domains, including two different types of MT-binding modules with overlapping Ca²⁺/calmodulin-binding motifs, 3 Mn modules with a consensus sequence (S(T)XXXXD(E)F(Y)RAWXXXR(K)) and 1-6 mammal-specific Mc modules or central repeats (species-dependent repeat numbers)¹⁵⁻¹⁷. Mn modules stabilize MTs against cold- and nocodazole-induced depolymerization, whereas Mc modules only bind and stabilize MTs at cold, as well as interact with actin^{15,18}. Despite its critical role in stabilizing MTs and broad expression in brain cells, MAP6 knockout (KO) mice are surprisingly viable, but display behavioral alterations in motor activity, cognition, and emotion, reminiscent of characteristic symptoms of schizophrenia^{15,19,20}. However, the molecular mechanisms and neural substrates underlying these behavioral alterations in MAP6 KO mice remain unclear.

Kv3.1 has been implicated in the diagnosis and treatment of schizophrenia^{10,11}. Kv3.1 channel belongs to the Kv3 subfamily whose members open at more positive potentials (~-10 mV), very rapidly activate and deactivate in response to changes in voltage, enabling neurons to fire action potentials at

high frequencies²¹⁻²⁴. Kv3.1 channel proteins are highly expressed in multiple types of neurons in the brain, including parvalbumin-positive (PV+) GABAergic interneurons in the cortex and hippocampus^{22,25}. Its mutations have been linked with epilepsies, intellectual disability, and encephalopathies²⁶⁻³⁰. Our early studies identified new binding partners of this channel regulating its axonal targeting^{31,32}, but how Kv3.1 channel proteins are regulated to affect behavior remains poorly understood.

In the present study, we have found that MAP6 and Kv3.1 proteins actually directly bind through the Mn modules and N-terminal T1 domain. This binding appears conserved in fast-spiking GABAergic interneurons in multiple brain regions, consistent with the fact that their KO mice show similar hyperactivity and reduced risk avoidance. Using stereotaxic microinjection of AAV-shRNA to knock down MAP6 in different brain regions, we identified that the amygdala and hippocampus are separately involved in regulating risk avoidance, long-term recognition memory, and hyperactivity. Our *in vivo* results of Kv3.1 knockdown and MAP6-Kv3.1 binding disruption support that these effects of MAP6 knockdown are mainly through altering Kv3.1 channels.

Results

Behavioral alterations caused by MAP6 or Kv3.1 gene deletion.

Several key behavioral changes in MAP6^{-/-} mice were consistently observed by multiple research groups and proposed to be used for modeling schizophrenia^{15,19,20,33}. Our results have further revealed striking similarities in behavioral alterations observed in MAP6^{-/-} and Kv3.1^{-/-} mice. The elevated plus maze (EPM) is a well-validated test of unconditioned anxiety-like behavior with decreased open arm time and open arm entries typically reflecting an anxiogenic phenotype. Interestingly, global deletion of MAP6 or Kv3.1 markedly increased the percentage time in open arms and total travel distance (Fig. 1a, b), indicating reduced risk avoidance or the opposite of an anxiogenic phenotype. In the open-field assay, a simple sensorimotor test used to determine general activity levels, gross locomotor activity, and exploration habits, both MAP6^{-/-} and Kv3.1^{-/-} mice displayed a marked increase of motor activity, compared to WT mice (Fig. 1c, d). These results in EPM and open-field tests were highly repeatable in our laboratory, and consistent with published results from other laboratories^{20,34}. These similarities in

behavioral alterations of the two KO mouse lines prompted us to perform additional behavioral assays for a more comprehensive comparison. The novel object recognition (NOR) task is used to evaluate long-term recognition memory, which is based on the spontaneous tendency of rodents to spend more time exploring a novel object than a familiar one. MAP6^{-/-} but not Kv3.1^{-/-} and WT mice showed unbiased time spent close to both the familiar and novel objects (Fig. 1e, f), indicating a deficit in long-term recognition memory in MAP6^{-/-} mice consistent with earlier results²⁰. The rotarod test measures coordination and motor skill learning, in which MAP6^{-/-} but not Kv3.1^{-/-} mice showed a clear reduction in time on the rotating rod compared to WT mice (Fig. 1g). Moreover, the balance beam test is used to assess fine motor coordination and balance in rodents, whereas Y maze spontaneous alternation is used to assess spatial working memory. In both tests, no significant difference was detected between the KO and WT mice (Fig. 1h, i). Therefore, both MAP6^{-/-} and Kv3.1^{-/-} mice displayed reduced avoidance and hyperactivity in the EPM and open-field tests, whereas only MAP6^{-/-} mice showed significant deficits in recognition memory revealed by the NOR test and motor skill learning revealed by the rotarod test (Fig. 1).

MAP6 deletion markedly reduces Kv3.1 protein levels in multiple brain regions

Since MAP6 and Kv3.1 KO mice displayed similar hyperactivity and avoidance reduction, we wondered how their proteins are expressed and distributed in the brain. Whereas MAP6 proteins are broadly expressed in the brain, Kv3.1 channels are mainly expressed in PV+ GABAergic interneurons in multiple brain regions^{15,19-22,25,35-37}. In the present study, we focus on the hippocampus, amygdala, and substantia nigra, which are involved in regulating memory, emotion, and motor activity. In the above-mentioned three regions, MAP6 and Kv3.1b channels highly colocalized in the somatodendritic region of Wisteria Floribunda Agglutinin-positive (WFA+) interneurons, which were the PV+ fast-spiking GABAergic interneurons (Figs. 2a-d and S1). MAP6 proteins appeared to preferentially concentrate in the cell body of Kv3.1+ and PV+ GABAergic interneurons (Fig. 2d), but not in the cell body of most pyramidal neurons. In these brain regions of heterozygous MAP6^{+/-} and homozygous MAP6^{-/-} mice,

Kv3.1 expression levels markedly reduced compared to its level in WT brains (Fig. S2). Using confocal microscopy, we further found that Kv3.1b channels were highly colocalized with MAP6 in the cell body and proximal dendrites of WFA+ interneurons in the WT brain, whereas both MAP6 and Kv3.1b largely eliminated from WFA+ interneurons in MAP6^{-/-} brain (Fig. 2e, f). In WT mice, Kv3.1b was found in PV+ axons of these brain regions, whereas Kv3.1b staining signals were largely absent in PV+ axons in the MAP6^{-/-} brain (Fig. 2g,h).

To further determine the MAP6 and Kv3.1 levels in the entire mouse brain, we performed the Western blotting analysis of the brain lysates from WT, MAP6^{+/-}, MAP6^{-/-}, and Kv3.1^{-/-} mice. MAP6 proteins were reduced by approximately 40% in MAP6^{+/-} brains and totally eliminated in MAP6^{-/-} brains, but did not change in Kv3.1^{-/-} brains (Fig. 2i, j). On the other hand, Kv3.1b proteins were reduced by approximately 60% in MAP6^{+/-} and MAP6^{-/-} brains and totally eliminated in Kv3.1^{-/-} brains (Fig. 2i, j). In sharp contrast, the total protein levels of Kv1.2 and Nav1.1 voltage-gated Na⁺ (Nav) channels remained the same in WT, MAP6^{+/-} and MAP6^{-/-} brains (Fig. S3). Thus, our Western blotting results are highly consistent with the immunostaining results. Taken together, MAP6 reduction selectively and drastically decreases the Kv3.1 channel level in PV+ GABAergic interneurons in the brain, which may give rise to various behavioral alterations in mice. These results have raised interesting questions regarding the relationship between MAP6 and Kv3.1, as well as the mechanism by which MAP6 deletion reduces the Kv3.1 protein level.

The first two Mn modules of MAP6 directly bind Kv3.1 channel

Our mass spectrometry analysis revealed multiple potential binding partners for Kv3.1 N-terminal fusion protein, including KIF5B³², as well as MAP6. However, these hits required further experimentation for verifying their direct binding to Kv3.1 and for determining the functional consequences of such binding. First, to confirm their interaction *in vivo*, we performed tissue co-immunoprecipitation (co-IP) using a specific anti-Kv3.1b antibody to pull down mouse brain lysates, followed by Western blotting using an

anti-MAP6 antibody. Indeed, the anti-Kv3.1b antibody pulled down MAP6 proteins from mouse brain lysates (Fig. 3a). To further map the Kv3.1 cytoplasmic domain mediating the binding, we fused GST to either N- or C-terminus from Kv3.1b or Kv1.2 (as control) to pull down MAP6N-GFP expressed in HEK293 cells. MAP6N-GFP was only pulled down by GST-31T1 (Fig. 3b, c). These results successfully verified the data from the early mass spectrometry analysis.

To map the Kv3.1-binding site in MAP6, we used GFP-fusion proteins of MAP6 truncations and 6×His-tagged major domains of MAP6N, which were pulled down by bacterially expressed and purified GST-31T1. MAP6E-GFP (missing the C-terminal domain), ΔPPP-GFP (missing the N-terminal Pro-rich domain), and ΔMc-GFP (missing the 5 Mc module repeats) were pulled down by GST-31T1 but not GST (Fig. 3d, e). Furthermore, His-MAP61 (aa 1-271), His-MAP62 (aa 36-271), and His-31T1, but not His-MAP63 (aa 222-451) and His-MAP64 (aa 452-615), were pulled down by GST-31T1 (Fig. 3d, f, g). To further pinpoint the binding site within MAP62 (aa 36-221), we made additional 6×His-tagged fusion proteins and found that the two Mn domains (aa 115-184) mediated the binding to Kv3.1 T1 domain (Fig. 3h, i). These two Mn modules are sufficient to stabilize MT *in vitro* against cold- or nocodazole-induced depolymerization¹⁶. Whereas each of the two Mn modules can binds MT or Ca²⁺/calmodulin¹⁶, both were required to bind the Kv3.1 T1 domain. Thus, both of the first two Mn domains (as well as their linker about 20 aa) of MAP6 are necessary and sufficient for the direct binding to the Kv3.1 T1 domain.

MAP6 can bind both monomeric and tetrameric Kv3.1 T1 domains with high affinity

To determine whether T1 tetramerization is required for MAP6 binding, we performed the pull-down assay in the presence and absence of 100 mM EDTA. We previously showed that EDTA can chelate Zn²⁺ to disassemble T1 tetramers into monomers, abolishing the binding between KIF5B tail domain and Kv3.1 T1 domain³². In contrast, the binding between MAP6 Mn modules and Kv3.1 T1 domain was largely retained in the presence of EDTA (Fig. 4a, b), suggesting that MAP6 can bind Kv3.1 T1 monomers. We further examined the roles of three point mutations of the Kv3.1 T1 domain required for coordinating a Zn²⁺ cation (Fig. 4c, d). Our results showed that two T1 mutants, His-H77A and His-

C2A2 (both C104 and C105 mutated to A), no longer bound the MAP6 Mn modules, whereas the third T1 mutant His-C83A (on the interface different from H77, C104, and C105) still bound (Fig. 4d, e). This is different from KIF5B binding to the T1 domain, in which all three mutants lost the binding³². Thus, these results have confirmed that MAP6 Mn modules can bind Kv3.1 T1 monomers and that the T1 interface containing H77 and C104 is required to generate a functional binding surface for MAP6.

To assess the binding affinity between Kv3.1 T1 domain and MAP6 Mns, we purified the two fusion proteins, His-31T1 and GST-M115-221, and used them in the pull-down assay. We found that GST-M115-221 efficiently pulled down purified His-31T1 revealed by the colloidal blue staining (Fig. 4f). Next, we used surface plasmon resonance (SPR) to determine the binding affinity between them. Purified His-31T1 proteins were covalently linked to the chip surface, while we flowed the solution containing different concentrations of GST-M115-221 over the coated surface (Fig. 4g). The K_d between GST-M115-221 and His-31T1 was calculated as 62.5 ± 18.4 nM, representing a high-affinity binding.

MAP6 stabilizes Kv3.1b channel proteins in neuronal soma and axonal terminals

To determine how MAP6 may regulate Kv3.1 channel localization in neurons and *vice versa*, we transfected HA-tagged Kv3.1b (Kv3.1bHA), MAP6N-GFP, or their mutants into cultured hippocampal neurons at 6 days *in vitro* (DIV). At 6 DIV when these cultured neurons are between stages 4 and 5 as previously described³⁸, they express endogenous MAP6 proteins, but not Kv3.1 channels^{23,39}. When co-expressed in these young neurons, Kv3.1bHA and MAP6N-GFP were highly colocalized in the cell bodies, axons, and axonal terminals (Fig. 5a, b). The mutant Kv3.1bHA_{H77} (H77 within the T1 domain mutated to A), no longer binding to MAP6, was restricted in the cell body with a low overall expression level, while MAP6N-GFP was mainly localized into axons (Fig. 5c, d). The mutant of Kv3.1 ATM, Kv3.1bHA_{KKK} (3 Ks within the C-terminal ATM mutated to 3 As), no longer present in axons but retaining the binding to MAP6, remained in the somatodendritic regions in the presence of MAP6N-GFP, and trapped MAP6N-GFP in the cell body (Fig. 5e, f). When co-expressed with MAP6Δ1-GFP (missing aa 1-36 in MAP6), which lost the axonal localization motif in the N-terminus, Kv3.1bHA proteins were also

restricted in the cell body and highly colocalized with MAP6 Δ 1-GFP (Fig. 5g, h). The colocalization between Kv3.1bHA_{KKK} and MAP6N-GFP, as well as between Kv3.1bHA and MAP6N Δ 1-GFP, resembled the interaction between endoplasmic reticulum and microtubules in the cell bodies (Fig. 5f, h). Taken together, our cell biology data suggest that MAP6 can stabilize Kv3.1 channels in both the cell body and axons of neurons. Without MAP6, Kv3.1b channels may be trapped within the endoplasmic reticulum and subsequently degraded, leading to protein level reduction. On the other hand, the presence of Kv3.1b channels in the soma helps to retain MAP6 there, which may explain why endogenous MAP6 proteins were preferentially concentrated in the soma of Kv3.1-expressing GABAergic interneurons (Fig. 2b-d).

Knocking down MAP6 in the amygdala specifically reduces risk avoidance behavior and Kv3.1b channel expression

To determine the neural circuit(s) mediating the impact of MAP6 deletion on mouse behavior, we used AAV-shRNA to knock down endogenous MAP6 protein in different brain regions. We designed the shRNA probes for MAP6 and made AAV9 viral particles with VectorLabs. First, we injected AAV-MAP6-shRNA or AAV-control-shRNA into the amygdala (AP: -1.5 mm; ML: -3.2 mm; DV: -5.0 mm) of WT B6 mice (Fig. 6a, b). Four weeks after injection, we performed a battery of behavioral assays. The mice that received AAV-MAP6-shRNA but not AAV-control-shRNA in the amygdala displayed a drastic reduction of risk avoidance, reflected by an increased percentage of open-arm time in EPM and center time in open field (Fig. 6c-e). These results replicated avoidance reduction displayed in MAP6^{-/-} and Kv3.1^{-/-} mice (Fig. 1). Interestingly, these injected mice displayed no clear change in recognition memory, overall motor activity, motor coordination and skill learning, and working memory in the NOR, open-field, rotarod, balance beam, and Y maze assays (Fig. 6c-i). Taken together, knocking down MAP6 in the amygdala specifically causes avoidance reduction but not other behavioral changes displayed in MAP6^{-/-} mice.

Therefore, MAP6 deletion causes risk avoidance reduction likely by disrupting the neural circuit in the amygdala.

To determine whether MAP6 knock down indeed reduced the level of Kv3.1b channel proteins, we performed immunostaining to assess the levels of endogenous MAP6 and Kv3.1b proteins. Kv3.1b channels are mainly expressed in the basolateral amygdala with a much lower level in the central nucleus³⁶. Based on the GFP expression, some neurons in the amygdala were indeed infected in the mouse brains injected with either AAV control shRNA or AAV MAP6 shRNA. We focused our analysis on GFP+ infected neurons. Some GFP+ neuronal cell bodies expressed high levels of MAP6 and Kv3.1b in the amygdala with AAV control shRNA, whereas many GFP+ neuronal cell bodies did not contain staining signals for MAP6 and Kv3.1b (Fig. 6j, k). This result is consistent with the fact that Kv3.1b expression is restricted in PV+ GABAergic interneurons in the basolateral amygdala and our data that MAP6 is preferentially concentrated in Kv3.1b+ cell bodies (Fig. 2d). Confocal imaging further showed that GFP+ and MAP6+ neurons with control shRNA expressed Kv3.1b in the soma and axons, but the GFP+ neuron with MAP6 shRNA did not express MAP6 and Kv3.1b (Fig. 6l). It is important to note that a GFP- neuron (an uninfected neuron indicated by a white asterisk) expressed both MAP6 and Kv3.1b under the AAV-MAP6-shRNA condition (Fig. 6l bottom). The quantification clearly showed that knocking down MAP6 led to marked reduction of Kv3.1b channel protein level in the amygdala (Fig. 6m), consistent with our results from KO mice and *in vitro* binding analysis. Taken together, our results support that MAP6 deletion in Kv3.1b+ and PV+ GABAergic interneurons in basolateral amygdala reduced the Kv3.1b level, which may result in risk avoidance reduction as observed in MAP6 and Kv3.1 KO mice.

Knocking down MAP6 in the hippocampus impairs recognition memory and causes hyperactivity

To test the role of the hippocampus in MAP6 deletion-mediated behavioral changes, we injected AAV-MAP6-shRNA or AAV-control-shRNA into the hippocampus (AP: -2.8 mm; ML: -3.0 mm; DV: -3.0 mm) of WT B6 mice. Four weeks after the injection, we performed the behavioral assays. The mice that

received AAV-MAP6-shRNA but not AAV-control-shRNA in the hippocampus displayed significant impairment of recognition memory in NOR and increased mobility in the open-field test (Fig. 7a-d), consistent with the behavioral alterations of MAP6^{-/-} mice. Interestingly, these injection mice showed no change in risk avoidance in EPM, motor function in rotarod, motor coordination in balance beam, and working memory in Y maze (Fig. 7e-h). Although knocking down MAP6 in hippocampal neurons likely causes increased motor activity through reducing Kv3.1 channel level, the long-term memory deficit observed in the mice injected with AAV-MAP6-shRNA in the hippocampus likely involves an additional mechanism. This is because Kv3.1^{-/-} mice display hyperactivity in open field but not recognition memory deficit in NOR (Fig. 1).

Similar to our analysis in the amygdala, we further verified the effects of MAP6 knockdown on Kv3.1b expression in infected hippocampal neurons. We found that endogenous MAP6 and Kv3.1 expression levels were markedly reduced in GFP⁺ neurons infected by AAV-MAP6-shRNA but not by AAV-control-shRNA in the hippocampus (Fig. S4).

Increased activity of projection neurons by MAP6 knockdown in the hippocampus and amygdala

To determine the impact of MAP6 knockdown on the activity of neural circuitry in the hippocampus and amygdala, we performed immunostaining using a specific anti-ΔFosB antibody followed by fluorescence microscopy. ΔFosB is an activity-dependent transcription factor in the immediate early gene family and has a long half-life that allows it to accumulate in chronically active neurons⁴⁰. In the AAV-control-shRNA brain, the overall ΔFosB signals were low and sparse in the hippocampus, but many PV⁺ interneurons had a higher level of ΔFosB signals, suggesting that PV⁺ fast-spiking GABAergic interneurons are relatively more active under normal conditions. In contrast, in the AAV-MAP6-shRNA brain, ΔFosB signals significantly increased in CA3 pyramidal neurons surrounding those infected neurons in the hippocampus (Fig. 7i-l). Similarly, PV⁻ projection neurons surrounding the neurons infected with AAV-MAP6-shRNA appeared to express higher levels of ΔFosB in basolateral

amygdala, and this effect was not present in the AAV-control-shRNA amygdala (Fig. 7j). Taken together, our results suggest that MAP6 knockdown may suppress the firing rate of PV+ GABAergic interneurons through downregulating Kv3.1b channels and hence lead to aberrantly high activation of CA3 pyramidal neurons in the hippocampus or projection neurons in basolateral amygdala. The increased activation of projection neurons in the amygdala and hippocampus may in turn lead to behavioral alterations, reduced risk avoidance, and hyperactivity/recognition memory deficit, respectively.

Kv3.1 Knockdown or MAP6-Kv3.1 binding disruption in the amygdala or hippocampus causes avoidance reduction and hyperactivity

To confirm that the effects of MAP6 deletion on behavior are mainly mediated by Kv3.1 reduction, we performed AAV-Kv3.1-shRNA (AAV-control-shRNA as control) stereotaxic injection into the amygdala (AP: -1.5 mm; ML: -3.2 mm; DV: -5.0 mm) or hippocampus (AP: -2.8 mm; ML: -3.0 mm; DV: -3.0 mm) of WT mice. We performed behavioral assays four weeks after injection. Knocking down Kv3.1 in the amygdala resulted in an increased percentage of the open-arm time in EPM and of the center time in open field (Fig. 8a,b), consistent with the results of MAP6 knockdown in the amygdala (Fig. 6b-e). Knocking down Kv3.1 in the hippocampus markedly increased the mobility in open field (Fig. 8c,d), consistent with the results of MAP6 knockdown in the hippocampus (Fig. 7d). Moreover, Kv3.1 knockdown in either the hippocampus or amygdala did not affect recognition memory in the NOR test (Fig. 8e), which is different from the result of MAP6 knockdown in the hippocampus (Fig. 7b,c), but consistent with the result in Kv3.1^{-/-} mice (Fig. 1e,f). Kv3.1 knockdown in the two regions did not alter motor coordination and skill learning, and working memory, in the rotarod, balance beam, and Y maze tests (data not shown). After behavioral testing, we stained the mouse brains to evaluate the knockdown efficiency of AAV-Kv3.1-shRNA and found that Kv3.1b⁺ cells were largely absent in either injected amygdala or injected hippocampus (Fig. 8f,g). Our confocal imaging further showed the presence or absence of Kv3.1b signals in PV+ interneurons infected by AAV-control-shRNA or AAV-Kv3.1-shRNA in the hippocampus, respectively (Fig. 8h,i).

To assess the effects of disrupting the MAP6-Kv3.1 binding on behavior, we cloned GFP-M115-221 (GFP-Mn) containing the first two Mn modules into AAV expression vector as described in our previous paper⁴¹, and performed AAV-GFP-Mn (AAV-GFP as control) stereotaxic injection into the amygdala or hippocampus of WT mice. Expression of GFP-Mn in the amygdala increased the percentage of open-arm time in EPM, as well as the mobility, but not the center time in open field (Fig. S5a,b). Expression of GFP-Mn in the hippocampus markedly increased the mobility in the open-field and EPM tests (Fig. S5c,d). Again, GFP-Mn expression in either the hippocampus or amygdala did not affect recognition memory in the NOR test (Fig. S5e), motor coordination and skill learning in rotarod and balance beam, and working memory in Y maze (data not shown). GFP-Mn expression did not alter the density of Kv3.1b+ cells in injected brain regions, including the amygdala and hippocampus (Fig. S5f,g). The Kv3.1b level in the soma of GFP+ and PV+ interneurons remained unchanged (Fig. S5h-j), whereas the Kv3.1b level in the axons inversely correlated with the GFP intensity (Fig. S5k-m), indicating that GFP-Mn reduced the axonal level of Kv3.1b. Thus, these findings support that MAP6 disruption causes risk avoidance reduction and hyperactivity mainly through Kv3.1 suppression.

Discussion

In the present study, we have identified a novel direct binding between a microtubule-binding protein MAP6 and Kv3.1 K⁺ channel, which is mediated by the first two Mn modules of MAP6 and Kv3.1 N-terminal T1 domain (Fig. 3). Different from KIF5B's exclusive binding to Kv3.1 T1 tetramers³², MAP6 binds T1 monomers as well (Fig. 4). This binding is required for stabilizing Kv3.1b channels in the soma and axons. Strong colocalization between MAP6 and Kv3.1b in intracellular networks in the soma suggests that their binding may in part mediate the interaction between the endoplasmic reticulum and microtubules. This can further allow Kv3.1 channel proteins to be trafficked out of the endoplasmic reticulum in the secretory pathway. Without the MAP6 binding, Kv3.1b channels may be trapped within the endoplasmic reticulum and get degraded later. This notion is consistent with our results from MAP6 KO mice (Fig. 2). The possibility that Kv3.1b reduction in the KO mice may result from protein synthesis inhibition was eliminated by our results from AAV-shRNA mediated knockdown in adult mice (Figs. 6, 7).

Moreover, MAP6-Kv3.1 interaction might be quite dynamic, since we previously showed that Kv3.1 C-terminal axonal targeting motif (ATM) directly binds its T1 domain³¹, which was confirmed by a recent structural study²⁴. Interestingly, this ATM also binds ankyrin-G³¹. The binding affinity between MAP6 Mn modules and Kv3.1 T1 domain is quite high with a Kd around 60 nM (Fig. 4f.g), which is in a similar range to the binding affinity between KIF5B tail and Kv3.1 T1³². The Kd between the two Mn modules and two Ca²⁺/calmodulin molecules was determined to be around 400 nM¹⁶. Taken together, these results appear to point to a MT- and Ca²⁺-dependent membrane trafficking and axonal targeting of Kv3.1 channel proteins. How these interactions regulate Kv3.1 channel proteins to exit from the endoplasmic reticulum and traffic through the Golgi to reach the plasma membrane in the cell body, as well as to target to axonal terminals, remain to be determined in future investigations.

MAP6 is required for maintaining the normal level of risk avoidance and motor activity through stabilizing Kv3.1b channel levels in PV+ GABAergic interneurons in the amygdala and hippocampus. Our results showed that MAP6^{-/-} and Kv3.1^{-/-} mice, as well as the mice injected with AAV-MAP6-shRNA in the amygdala displayed risk avoidance reduction but not other behavioral changes (Figs. 1, 6), suggesting that Kv3.1b reduction in the amygdala specifically causes avoidance reduction. On the other hand, MAP6 knockdown in the hippocampus specifically caused hyperactivity, consistent with the effects of both MAP6^{-/-} and Kv3.1^{-/-} mice, suggesting MAP6-induced Kv3.1 reduction in the hippocampus leads to hyperactivity. However, recognition memory deficit in NOR was observed in MAP6^{-/-} mice and AAV-injected mice in the hippocampus, but not in Kv3.1^{-/-} mice. This result suggests that MAP6 deletion may change other neuronal function that does not involve Kv3.1. For instance, two other members of the Kv3 subfamily, Kv3.3 and Kv3.4, are expressed in the mossy fiber of dentate granule cells⁴². Since the T1 domains of Kv3.1, Kv3.3 and Kv3.4 are highly homologous to each other, MAP6 deletion may reduce their levels in the mossy fiber as well, leading to the behavioral alterations that are not present in Kv3.1 KO mice. Furthermore, other binding partner(s) of MAP6 might be involved in such alteration. In the present studies, we focused on the amygdala and hippocampus. How other brain regions are involved in MAP6-Kv3.1 mediated changes remains to be determined in future studies.

How does MAP6 knockdown affect the overall activity of neural circuitry in the hippocampus and amygdala? The Δ FosB staining data indicated a marked increase of CA3 pyramidal neurons (Fig. 7i-l), which might be partially caused by disinhibition due to reduced firing from PV+ and inhibitory GABAergic interneurons (Fig. S6a). Hyperexcitability of CA3 pyramidal neurons disrupts pattern separation and pattern completion in the hippocampal neural circuit, and has been associated with hyperactivity and recognition memory deficit⁴³⁻⁴⁵. On the other hand, marked reduction of Kv3.1 levels in PV+ GABAergic interneurons could increase the excitability of projection neurons in basolateral amygdala as shown by Δ FosB staining (Fig. 7j). This increased activity might in turn stimulate the inhibitory neurons in central amygdala to reduce risk avoidance or anxiety-like behavior in a bidirectional circuit (Fig. S6b)⁴⁶. It is important to note that one-sided injection was performed in every mouse in all of our experiments, which was sufficient to cause specific behavioral changes. GFP signals were present in the contralateral amygdala, hippocampus, or other regions (Figs. 6a, 7a lower panels), but most of these GFP signals were from thin neuronal processes, indicating the axons projected from infected neurons in the ipsilateral amygdala or hippocampus. Thus, the single-sided injection still affects both sides. Furthermore, it is possible that a small percentage of injected AAV particles may diffuse to the brain regions adjacent to the injection site. Our post hoc analysis confirmed that most infected neuronal cell bodies were confined with the intended brain region. Nonetheless, our findings suggest that neural circuits show different levels of vulnerabilities to alterations of PV+ fast-spiking GABAergic interneurons, resulting in a behavioral change. For instance, the normal level of risk avoidance and motor activity appears to require proper firing rate of PV+ GABAergic interneurons in the amygdala and hippocampus. In contrast, normal long-term recognition memory might perhaps mainly rely on the trisynaptic connections of excitatory neurons but not the fast spiking of PV+ GABAergic interneurons in the hippocampus.

Knockdown of Kv3.1 or disrupting the MAP6-Kv3.1 binding in the amygdala or hippocampus led to avoidance reduction and hyperactivity (Figs. 8 and S5), supporting our hypothesis that the behavioral effect of MAP6 deletion is mainly mediated by Kv3.1 suppression. Of note, the two injections in the amygdala also moderately increased the total moving distance in EPM but not in open field besides marked avoidance reduction, whereas the two injections in the hippocampus also decreased avoidance

in one of the two assays besides marked increases of moving activity in open field (Figs. 8a-d and S5a-d). Thus, although their behavioral effects were not as highly segregated in the amygdala and hippocampus as those of MAP6 knockdown (Figs. 6 and 7), the differential impact remains consistent. It is also important to note that the overall effect of Kv3.1 knockdown on behavior appeared more pronounced than the effect of GFP-Mn expression, which is consistent with their difference in affecting Kv3.1 channel proteins (Figs. 8 and S5).

Our results suggest that different types of alterations of PV+ interneurons may affect behavior differently. For instance, SCN1A or Nav1.1 channels are specifically expressed in PV+ GABAergic interneurons, and SCN1A^{-/+} mice display hyperactivity in the open-field test⁴⁷, similar to Kv3.1^{-/-} mice. However, contrary to Kv3.1^{-/-} mice, SCN1A^{+/-} mice showed increased anxiety-like behavior as indicated by reduced open-arm time in EPM⁴⁷. Although both Nav1.1 and Kv3.1 channels are required for the proper firing of PV+ GABAergic interneurons, their reduction have different effects. Nav1.1 deletion inhibits action potential firing in general, whereas Kv3.1 deletion only reduces fast spiking but not regular firing of action potentials. Regular action potential firing is actually supported by Kv1 channels expressed in PV+ GABAergic interneurons²³. Therefore, extensive investigations in this direction will provide a deeper understanding of the regulations of these interneurons and may allow us to develop novel strategies to manipulate their activities to influence behavior. For instance, future studies regarding the role of MAP6-Kv3.1 interaction in PV+ GABAergic interneurons of the medial prefrontal cortex should provide new mechanistic insights into social interactions.

Finally, our findings have unraveled a novel physical binding between MAP6 and Kv3.1. Their dysfunctions, among other many proteins, were previously implicated in the pathogenesis of mental disorders, especially schizophrenia⁵⁻¹¹. It remains unknown why so many risk genes are involved in mental disorders. Our findings suggest that a better understanding of the functional relationship of these risk genes, as well as their distinct impact on behavior, may be necessary to discover the core pathogenic mechanism across multiple levels (e.g. molecule, cell, and neural circuitry), and will certainly contribute to the development of new rationale therapies to combat these devastating disorders.

Methods

Antibodies

Mouse monoclonal antibodies: the anti-MAP6 antibody (STOP (175), mAb #4265, Cell Signaling Technology, Inc), anti-Kv3.1b antibody (N16B/8, NeuroMab), anti-GFP antibody (N86/8, NeuroMab), anti-6xHis antibody (N144/14, NeuroMab), anti-Parvalbumin antibody (L114/81, NeuroMab), anti-Nav1.1 antibody (K74/71, NeuroMab), and anti-Kv1.2 antibody (K14/16, NeuroMab). The rabbit monoclonal antibody: anti-Delta FosB (D3S8R) antibody (mAb #14695, Cell Signaling Technology, Inc). Rabbit polyclonal antibodies: the anti-MAP6 antibody (NBP214220, Novus Biologicals), and anti-Kv3.1b (KCNC1) antibody (APC-014, Alomone labs). Secondary antibodies: AffiniPure Donkey Anti-Mouse IgG (H+L) Horseradish Peroxidase (715-035-151, Jackson ImmunoResearch Inc), AffiniPure Donkey Anti-Mouse IgG (H+L) Alexa Fluor® 594 (715-585-151, Jackson ImmunoResearch Inc), AffiniPure Donkey Anti-Mouse IgG (H+L) Alexa Fluor® 647 (715-605-151, Jackson ImmunoResearch Inc), AffiniPure Donkey Anti-Rabbit IgG (H+L) Horseradish Peroxidase (711-035-152, Jackson ImmunoResearch Inc), AffiniPure Donkey Anti-Rabbit IgG (H+L) Alexa Fluor® 594 (711-585-152, Jackson ImmunoResearch Inc), and AffiniPure Donkey Anti-Rabbit IgG (H+L) Alexa Fluor® 647 (711-605-152, Jackson ImmunoResearch Inc).

Maintenance of knockout (KO) mouse lines and genotyping procedures

All animal experiments have been conducted in accordance with the NIH Animal Use Guidelines and were approved by the Ohio State University Institutional Animal Care and Use Committee (IACUC). The MAP6^{-/-} mouse line was kindly provided by Dr. Annie Andrieux¹⁹ and maintained with heterozygous MAP6^{+/-} breeding pairs. MAP6^{+/-};Thy1-YFP and MAP6^{-/-};Thy1-YFP were obtained by crossing the MAP6^{+/-} and Thy1-YFP-H transgenic mice (The Jackson Laboratory #003782). These mouse lines have been maintained using a PCR-based genotyping procedure. The following primers were used for MAP6 KO: reverse primer (for both WT and MAP6 KO, 5'-CTGGGAAAACCACTGTGGAACTGTTA-3'), forward primer 1 (for WT, 5'-GCAGATGCCCTCAACAGGCAAATCCGG-3'), and forward primer 2 (for MAP6 KO, 5'-GATTCCCACCTTTGTGGTTCTAAGTACTG-3'). WT band: 270 bp. Mutant band: 400 bp.

For Thy1-YFP-H transgenic mice, forward primer (oIMR-1258): 5'-TCTGAGTGGCAAAGGACCTTAGG-3'; reverse primer (oIMR-1260): 5'-CGCTGAACTTGTGGCCGTTTACG-3'. Band size: 300 bp. The Kv3.1^{-/-} mouse line was originally provided by Dr. Ralf Joho at UT Southwestern Medical Center, backcrossed with C57BL/6 for more than 10 generations, and used in our recently published paper⁴⁸. The following primers were used for genotyping the Kv3.1^{-/-} mouse line: forward primer 31 F775 (for both WT and KO, 5'-GCGCTTCAACCCCATCGTGAACAAGA-3'), reverse primer 31R991 (for WT, 5'-GGCCACAAAGTCAATGATATTGAGGG-3'), and reverse primer PNR278 (for KO, 5'-CTACTTCCATTTGTCACGTCCTGCAC-3').

Mouse behavioral assays

The elevated plus maze (EPM) test was described in detail in our recent paper⁴⁹. In brief, EPM testing was carried out on a raised (74 cm) plus-shaped maze with four arms (34 cm long). Two opposite arms were “open” with no walls; the other two arms were “closed” by opaque walls (22 cm high). Mice were placed in the center of the maze at the intersection of the two arms and allowed to explore the maze for 5 min. Total distance traveled, arm entries, and time spent on the four arms were recorded, with the percentage time spent in the open arms ($100 \times T_{\text{Open}} / (T_{\text{Open}} + T_{\text{Closed}})$) of the EPM used as a measure of anxiety-like or risk avoidance behavior. Time spent in the center was not included in the analysis.

The open-field test was described in detail in our recent paper⁴⁹. Each mouse was placed in the center of a square arena (40 cm × 40 cm) and its behavior was recorded for 5 min. The total distance traveled was used as a measure of locomotion, and the ratio of time spent in the center (25 cm × 25 cm) and perimeter of the arena was used for assessing risk avoidance behavior.

The Y-maze test was described in detail in our recent paper⁴⁹. Each mouse was placed at the end of one arm of a symmetric Y maze with arms measuring 40 cm long, 8 cm wide, and 20 cm high and allowed 5 min to freely explore the apparatus. The series of arm entries (e.g. ACBCABCBCA) was recorded using an overhead camera. An alteration is counted when the mouse entered the 3 different arms during a triad on overlapping triplet sets. Spontaneous alternation was measured by counting the

number of times the mouse entered each of the 3 arms of the maze in succession divided by the maximum number of possible alternations and used to represent working memory.

The rotarod test was performed with Panlab 76-0770 (Barcelona, Spain) as described by the manufacturer. The setup contained a textured rod, which slowly rotated at 4 rpm at the beginning such that the mice had to walk at a matching pace to avoid falling off. In each 5-minute trial, the rod accelerated from 4 rpm to 40 rpm (increment at 7.2 rpm/min). The mouse must learn to adjust to the speed of the rod to avoid falling to the floor 10 cm below. The inter-trial interval was approximately 15 minutes. The amount of time the mouse was able to stay upright on the rotarod was used as a measure of motor function, and improved performance across trials was used as an indicator of motor learning.

The balance-beam test was performed using a flat metal beam (5 mm wide beam) mounted 1 meter above a tabletop via two platforms attached to ring stands. A mouse was placed on the beam on an open platform facing an enclosed box at the other end of the beam. The mouse was given 1 minute to traverse the beam before being guided to the goal box by the experimenter. Slips and/or falls from the beam, as well as gait, were recorded by a side-mounted camera. Mice will receive up to five trials on the beam. The inter-trial interval was 10 min. Padding was provided below the apparatus to reduce impact in the case of falling from the beam. The balance beam task served as a measure of vestibular function and motor coordination. Over the course of training, reduced time to traverse the beams also served as a measure of motor learning.

The novel object recognition (NOR) test was performed for assessing long-term recognition memory. In the open field arena, the objects to be discriminated were made of biologically neutral materials and attached to the bottom to prevent movement. Each mouse was given 5 minutes to explore two identical objects in the arena before being returned to its home cage. Four hours later, one of the two objects was replaced with a novel object and the mouse was reintroduced into the arena for 5 min. The ratio of time spent exploring the novel object over the familiar one serves as an indicator of long-term recognition memory.

Cardiac perfusion, fixation, and immunostaining

We have described the procedures of cardiac perfusion, fixation, sectioning, staining, and imaging in detail in our published papers^{39,41,48,50,51}. In brief, mice (3–5 months old) were anesthetized with Ethasol (Virbac; 100 mg/kg) and were transcardially perfused with 20 ml of PBS followed by 20 ml of a 4% formaldehyde/PBS solution. Then, mouse brains were removed, post-fixed for 1 h in 4% formaldehyde/PBS solution, cut into 3 mm blocks using an acrylic brain matrix (Braintree Scientific, Braintree, MA, USA), and cryoprotected in a 30% sucrose/PBS solution for 1–3 days. Brain blocks were embedded in optimal cutting temperature (OCT) media (Sakura Finetek USA, Inc., Torrance, CA, USA) and were stored at –80 °C until sectioning. We used a Microm HM550 cryostat (Thermo Scientific, Waltham, MA, USA) to cut brain blocks into 40- μ m-thick slides that were then collected on Superfrost Plus microscope slides (FisherScientific, Pittsburgh, PA, USA) for storage at –20 °C. After immunostaining, we mounted the sections with glass coverslips using tris-buffered Fluoro-Gel mounting media (Electron Microscopy Sciences, Hatfield, PA, USA).

Conventional fluorescence microscopy and confocal microscopy

Low magnification fluorescence images were captured with a Spot CCD camera RT slider (Diagnostic Instruments) in a Zeiss upright microscope, Axiophot, using Plan Apo objectives 20 \times /0.75 and 100 \times /1.4 oil, saved as 16-bit TIFF files, and analyzed with NIH ImageJ and SigmaPlot 14.0 for fluorescence intensity quantification and colocalization, as previously described^{32,39,49,51}. Exposure times were controlled so that the pixel intensities within the image field were below saturation, but the same exposure time was used for each fluorophore in an experiment. Fluorescence confocal microscopy and image stack capturing were carried out using Zeiss LSM 900 confocal system (Carl Zeiss AG, Oberkochen, Germany) with Airyscan SR. Images(.czi file) were taken using Zeiss 63 \times oil objectives (numerical aperture at 1.40) with ZEN 3.0 (blue edition) software. We captured Z-stack images at ~0.20 μ m steps for the selected areas of interest. Image stacks were analyzed with NIH ImageJ. Staining and imaging have been replicated at least for 3 rounds.

cDNA plasmids

Kv3.1bHA, Kv3.1bHA_{H77A}, Kv3.1bHA_{KKK}, GST-31T1, GST-31aC, GST-12N, GST-12C, His-31T1, His-H77A, His-C2A2, His-C83A, and GST-KIF5BTail were published in our papers^{31,32}. MAP6N-GFP (aa 1-952), MAP6E-GFP (aa 1-614), ΔMc-GFP, ΔPPP-GFP, and MAP6Δ1-GFP were kindly provided by Dr. Annie Andieux³⁵. His-MAP61 (aa 1-221), His-MAP62 (aa 36-221), His-MAP63 (aa 222-451), and His-MAP64 (aa 452-615) were constructed by inserting the corresponding PCR fragments into pRSET B between *Xho*I and *Hind*III. GST-M37-114 (aa 37-114 from MAP6N), GST-M115-221 (aa 115-221 from MAP6N), GST-M115-149 (aa 115-149 from MAP6B), GST-M141-184 (aa 141-184 from MAP6N), GST-M181-221 (aa 181-221 from MAP6N), and GST-M115-184 (aa 115-184 from MAP6N) were made by inserting the corresponding PCR fragments into pGEX4T-2 between *Xho*I and *Hind*III. AAV-GFP-M_N (aa 115-221 from MAP6N) was made by inserting the corresponding PCR fragment between *Acc*65I and *Bgl*III in scAAV-CMV-GFP.

Tissue co-immunoprecipitation (co-IP)

Tissue co-IP and Western blotting were prepared as previously described³². In brief, mouse brains were homogenized in homogenization buffer (50 mM Tris buffer, pH 8.0, 1 mM EDTA, and a Complete protease inhibitor tablet (Cat. #5892970001, Roche, Basel, Switzerland). Crude membranes were pelleted from the suspension by high-speed centrifugation at 10350 rpm for 30 min at 4°C, solubilized in IP buffer (50 mM Tris-Cl, pH 7.4, 150 mM NaCl, 1% Triton X-100, and a Complete protease inhibitor tablet) for 2 h at 4°C, and centrifuged at 10350 rpm for 30 min at 4°C. The supernatant (1 ml in each condition) was incubated (4 h, 4°C) with 40 μl of protein G-agarose beads (Cat. #11719416001, Roche, Basel, Switzerland) and 3 μl of mouse monoclonal anti-Kv3.1b antibody (Cat. #AB2877376, Neuromab, CA, USA), mouse monoclonal anti-MAP6 antibody (Cat. #4265, Cell Signaling Technology, Massachusetts, USA), or control mouse IgG (Sigma). The beads were washed six times with the IP buffer and eluted with 2× sample buffer. The immunoprecipitants were resolved by SDS-PAGE, transferred to a polyvinylidene difluoride membrane, and subjected to Western blotting with the mouse monoclonal anti-MAP6 antibody (1:1000 dilution). Each experiment was repeated 3 times with consistent results.

Protein pulldown assays and Western blotting

Procedures of protein pulldown assays and Western blotting were used as previously described^{31,32}. The expression of GST- or 6xHis-tagged proteins was induced with 1 mM Isopropyl β -D-1thiogalactopyranoside (IPTG) in *E. coli* BL21 cells for 4 h at 37°C. The bacterial pellets were solubilized with sonication in a pull-down buffer (50 mM Tris-HCl, pH 7.4, 150 mM NaCl, 1% Triton X100, and a Complete protease inhibitor tablet) at 4°C, and centrifuged at 10,350 $\times g$ for 30 min at 4°C. The supernatants were incubated with 50 μ l of glutathione beads at 4°C for 2 h. After extensive washing, the beads coated with purified GST fusion proteins were further incubated with either bacterial lysate supernatant containing 6xHis-tagged fusion proteins or the supernatant from HEK293 cells (CRL-1573, American Type Culture Collection) expressing GFP-tagged constructs. The proteins precipitated were eluted with a 2 \times sample buffer, resolved in SDS-PAGE, transferred to PVDF membrane, and subjected to immunoblotting with either an anti-His antibody (Cat. #AB2877254, Neuromab, CA, USA) or anti-GFP antibody (Cat. #AB2313651, Neuromab, CA, USA). The SDS-PAGE gels with GST fusion inputs were stained with the Colloidal Blue staining kit (Cat. #LC6025, Invitrogen, Massachusetts, USA). Protein pull down assay replication: 3 rounds. Western blot assay replication: 3 rounds. Mouse numbers are provided in the figures.

Visualization of the three-dimensional structure of Kv3.1 channel N-terminal tetramerization domain

We used the Protein Viewer plugin with the Virtual Studio code to visualize the published structure of the entire Kv3.1a channel²⁴ (PDB code: 7PHI). Here we focused on the N-terminal tetramerization domains with Zn²⁺-binding sites.

Surface plasmon resonance (SPR) for measuring the binding affinity between interacting proteins

The binding kinetics between purified GST-fused MAP6 Mn modules (GST-M115-221) and 6 \times His-tagged Kv3.1 T1 domain (His-31T1) was determined with the single and 2-channel OpenSPR

(Nicoya Lifesciences, Kitchener, ON). The assays were performed at room temperature with HBS running buffer (0.05% Tween-20, 2 mM CaCl₂, and 10% glycerol). Purified His-31T1 proteins were immobilized on a COOH chip with NHS/EDC activation. Purified GST-M115-221 proteins were diluted in HBS running buffer and subsequently injected for 5 min at a flow rate of 35 µl/min in a concentration series from 5 µg/ml to 100 µg/ml, with 7 min dissociation time. Sensors were regenerated with two injections of 10 mM HCl per regeneration step, with 40 sec contact time and 270 sec dissociation time. Sensorgrams were fitted with TraceDrawer analysis software (Ridgeview Instruments, Uppsala, Sweden). The SPR assay was repeated 2 times with consistent results.

Hippocampal neuron culture, transfection, and imaging

Hippocampal neuron culture was prepared as previously described^{41,52}. In brief, 2 d after neuron plating, 1 µM cytosine arabinose (Sigma) was added to the neuronal culture medium to inhibit glial growth for the subsequent 2 d, then replaced with the normal neuronal culture medium. The culture medium was replenished twice a week by replacing a half volume. For transient transfection, neurons in culture at 5–7 DIV were incubated in Opti-MEM containing 0.8 µg of cDNA plasmid and 1.5 µl of Lipofectamine 2000 (Invitrogen, Massachusetts, USA) for 20-30 min at 37°C. The procedures of immunocytochemistry and fluorescence microscopy were described previously^{39,41}. In brief, the transfected neurons expressing Kv3.1bHA (or its mutants) and MAP6N-GFP (or its truncation) were fixed, permeabilized, and stained with a rat monoclonal anti-HA antibody (Roche, Basel, Switzerland). Replicated times: 6 rounds of independent neuron culture and transfection.

AAV-shRNA knockdown of MAP6 and Kv3.1

Recombinant adeno-associated viral vectors (AAV) carrying the GFP and shRNA were used in this study. Candidate shRNA sequences were designed using siDirect 2.0, GenScript's siRNA Design Center, and siRNA-Finder. We focused on three shared sequences from different web sites and verified the knockdown efficacy for each in cultured hippocampal neurons.

For knocking down MAP6:

1: 5'-AAGGAGCAAAGCAAAGAGATGCTCGAGCATCTCTTTGCTTT GTCCTT-3';
2: 5'-CAACGAAGGGCACGAAGAGAACTCGAGTTCTCTTCGTGCCCTTCGTTG-3';
3: 5'-GGTAGAGAAACCTAGTGTTCACTCGAGTGAACACTAGGTTTCTCTACC-3'.

For knocking down Kv3.1:

1: 5'-GTGCCTGTCATCGTGAACAATCTCGAGATTGTTACGATGACAGGCAC-3';
2: 5'-TCGCTCACATCCTGAACTATTCTCGAGAATAGTTCAGGATGTGAGCGA-3';
3: 5'-GCTTCAACCCCATCGTGAACACTCGAGTGTTACGATGGGGTTGAAGC-3'.

The viruses were packaged and purified by the Vector Biolabs and Boston Children's Hospital virus core. Briefly, HEK293 cells were co-transfected with a capsidation plasmid (AAV9 serotype), a helper plasmid, and three different AAV-GFP-U6- shRNA plasmids containing GFP and shRNA sequences. The AAV were then isolated from the cell culture by ultracentrifugation and chromatography purification. The final preparation was tittered by real-time PCR and the concentration was 2.2×10^{12} vg/ml for MAP6 (7.64×10^{13} vg/ml for Kv3.1). AAV-scramble shRNA-GFP from Boston Children's hospital virus core is used as the control.

AAV-GFP-Mn

A recombinant adeno-associated viral vector (AAV) carrying the GFP-Mn was used in this study. The viruses were packaged and purified by Boston Children's Hospital virus core. Briefly, HEK293 cells were co-transfected with a capsidation plasmid (AAV9 serotype), a helper plasmid, and AAV-GFP-Mn plasmids. The AAV were then isolated from the cell culture by ultracentrifugation and chromatography purification. The final preparation was tittered by real-time PCR and the concentration was 4.46×10^{13} vg/ml .

Stereotaxic microinjection of AAV into different brain regions in mice

The surgery and microinjection procedures are similar to those described in earlier publication⁴¹. Briefly, mice were anesthetized with a mixture of 100 mg/kg ketamine and 20 mg/kg xylazine (Sigma-Aldrich, St. Louis, MO). Mice were mounted on a stereotaxic frame and a small straight incision was

made along the midline of the head to expose the underlying skull. The bregma coordinates were recorded and used as the reference point. The stereotaxic injection setup consisted of a Hamilton syringe connected to a 33 gauge injector cannula (Plastics One, Roanoke VA). A volume of 2-10 μ l of the virus was injected per mouse, at a rate of 0.1-0.25 μ l/min controlled by a syringe pump.

Microinjections of viral vectors were carried out to cover multiple regions, including the hippocampus (DV: -3.0 mm; AP: -2.8 mm; LR: -3.0 mm) and amygdala (DV: -5.0 mm; AP: -1.5 mm; LR: -3.2 mm). After the infusion was finished, the injector was left in place for 2 minutes before being raised. The mice were sutured after the surgery and administered post-operative care for one week. After four weeks of recovery, the GFP fluorescence was used to verify the injected brain region, AAV infection and MAP6/K α 3.1 knockdown. Four rounds of AAV injection were performed for this study.

Statistical analysis

Sample sizes were chosen based on our previous experiments and publications, as well as related literature in the field. No formal randomization was used to allocate samples to experimental condition. Whenever possible, the investigator was blind to the sample conditions. In AAV injection experiments, post hoc analyses of viral infection and protein expression were used to exclude the mice with no or incorrect AAV infection from behavioral results. Statistical analysis was conducted using SigmaPlot 15.0 software. To assess normality, the Shapiro-Wilk test was employed and the homogeneity of variances was evaluated using Brown-Forsythe tests. Results were presented as the mean \pm SEM. Two-tailed Student's t-test was used for comparisons between two groups. One-way ANOVA followed by Dunnett's test was used for comparing two or more groups to one control group. (*) $p < 0.05$, (**) $p < 0.01$, and (***) $p < 0.001$ were considered statistically significant.

References

1. Trubetskoy, V., Pardiñas, A.F., Qi, T., Panagiotaropoulou, G., Awasthi, S., Bigdeli, T.B., *et al.* Mapping genomic loci implicates genes and synaptic biology in schizophrenia. *Nature* **604**, 502-508 (2022).
2. Singh, T., Poterba, T., Curtis, D., Akil, H., Al Eissa, M., Barchas, J.D., *et al.* Rare coding variants in ten genes confer substantial risk for schizophrenia. *Nature* **604**, 509-516 (2022).
3. Schizophrenia Working Group of the Psychiatric Genomics, C. Biological insights from 108 schizophrenia-associated genetic loci. *Nature* **511**, 421-427 (2014).
4. Genovese, G., Fromer, M., Stahl, E.A., Ruderfer, D.M., Chambert, K., Landén, M., *et al.* Increased burden of ultra-rare protein-altering variants among 4,877 individuals with schizophrenia. *Nat Neurosci* **19**, 1433-1441 (2016).
5. Martins-de-Souza, D., Gattaz, W.F., Schmitt, A., Rewerts, C., Maccarrone, G., Dias-Neto, E., *et al.* Prefrontal cortex shotgun proteome analysis reveals altered calcium homeostasis and immune system imbalance in schizophrenia. *Eur Arch Psychiatry Clin Neurosci* **259**, 151-163 (2009).
6. Xiao, B., Xu, H., Ye, H., Hu, Q., Chen, Y. & Qiu, W. De novo 11q13.4q14.3 tetrasomy with uniparental isodisomy for 11q14.3qter. *Am J Med Genet A* **167A**, 2327-2333 (2015).
7. Shimizu, H., Iwayama, Y., Yamada, K., Toyota, T., Minabe, Y., Nakamura, K., *et al.* Genetic and expression analyses of the STOP (MAP6) gene in schizophrenia. *Schizophr Res* **84**, 244-252 (2006).
8. Wei, H., Sun, S., Li, Y. & Yu, S. Reduced plasma levels of microtubule-associated STOP/MAP6 protein in autistic patients. *Psychiatry Res* **245**, 116-118 (2016).
9. Chen, C.P., Lin, S.P., Chern, S.R., Wu, P.S., Chen, S.W., Wu, F.T., *et al.* Tetrasomy of 11q13.4-q14.3 due to an intrachromosomal triplication associated with paternal uniparental isodisomy for 11q14.3-qter, intrauterine growth restriction, developmental delay, corpus callosum dysgenesis, microcephaly, congenital heart defects and facial dysmorphism. *Taiwan J Obstet Gynecol* **60**, 169-172 (2021).
10. Yanagi, M., Joho, R.H., Southcott, S.A., Shukla, A.A., Ghose, S. & Tamminga, C.A. Kv3.1-containing K(+) channels are reduced in untreated schizophrenia and normalized with antipsychotic drugs. *Mol Psychiatry* **19**, 573-579 (2014).
11. Angelescu, I., Kaar, S.J., Reis Marques, T., Borgan, F., Veronesse, M., Sharman, A., *et al.* The effect of AUT00206, a Kv3 potassium channel modulator, on dopamine synthesis capacity and the reliability of [(18)F]-FDOPA imaging in schizophrenia. *J Psychopharmacol* **36**, 1061-1069 (2022).

12. Bosc, C., Cronk, J.D., Pirollet, F., Watterson, D.M., Haiech, J., Job, D., *et al.* Cloning, expression, and properties of the microtubule-stabilizing protein STOP. *Proceedings of the National Academy of Sciences of the United States of America* **93**, 2125-2130 (1996).
13. Job, D., Rauch, C.T. & Margolis, R.L. High concentrations of STOP protein induce a microtubule super-stable state. *Biochem Biophys Res Commun* **148**, 429-434 (1987).
14. Pirollet, F., Rauch, C.T., Job, D. & Margolis, R.L. Monoclonal antibody to microtubule-associated STOP protein: affinity purification of neuronal STOP activity and comparison of antigen with activity in neuronal and nonneuronal cell extracts. *Biochemistry* **28**, 835-842 (1989).
15. Cuveillier, C., Boulan, B., Ravanello, C., Denarier, E., Deloulme, J.C., Gory-Fauré, S., *et al.* Beyond Neuronal Microtubule Stabilization: MAP6 and CRMPs, Two Converging Stories. *Front Mol Neurosci* **14**, 665693 (2021).
16. Lefevre, J., Savarin, P., Gans, P., Hamon, L., Clément, M.J., David, M.O., *et al.* Structural basis for the association of MAP6 protein with microtubules and its regulation by calmodulin. *J Biol Chem* **288**, 24910-24922 (2013).
17. Bosc, C., Frank, R., Denarier, E., Ronjat, M., Schweitzer, A., Wehland, J., *et al.* Identification of novel bifunctional calmodulin-binding and microtubule-stabilizing motifs in STOP proteins. *J Biol Chem* **276**, 30904-30913 (2001).
18. Peris, L., Bisbal, M., Martinez-Hernandez, J., Saoudi, Y., Jonckheere, J., Rolland, M., *et al.* A key function for microtubule-associated-protein 6 in activity-dependent stabilisation of actin filaments in dendritic spines. *Nat Commun* **9**, 3775 (2018).
19. Andrieux, A., Salin, P.A., Vernet, M., Kujala, P., Julie Baratier, J., Gory-Fauré, S., *et al.* The suppression of brain cold-stable microtubules in mice induces synaptic defects associated with neuroleptic-sensitive behavioral disorders. *Genes & Development* **16**, 2350-2364 (2002).
20. Fournet, V., Schweitzer, A., Chevarin, C., Deloulme, J.C., Hamon, M., Giros, B., *et al.* The deletion of STOP/MAP6 protein in mice triggers highly altered mood and impaired cognitive performances. *Journal of Neurochemistry* **121**, 99-114 (2012).
21. Rudy, B. & McBain, C.J. Kv3 channels: voltage-gated K⁺ channels designed for high-frequency repetitive firing. *Trends Neurosci* **24**, 517-526 (2001).
22. Kaczmarek, L.K. & Zhang, Y. Kv3 Channels: Enablers of Rapid Firing, Neurotransmitter Release, and Neuronal Endurance. *Physiol Rev* **97**, 1431-1468 (2017).
23. Gu, Y., Servello, D., Han, Z., Lalchandani, R.R., Ding, J.B., Huang, K., *et al.* Balanced Activity between Kv3 and Nav Channels Determines Fast-Spiking in Mammalian Central Neurons. *iScience* **9**, 120-137 (2018).
24. Chi, G., Liang, Q., Sridhar, A., Cowgill, J.B., Sader, K., Radjainia, M., *et al.* Cryo-EM structure of the human Kv3.1 channel reveals gating control by the cytoplasmic T1 domain. *Nat Commun* **13**, 4087 (2022).

25. Weiser, M., Bueno, E., Sekirnjak, C., Martone, M.E., Baker, H., Hillman, D., *et al.* The potassium channel subunit KV3.1b is localized to somatic and axonal membranes of specific populations of CNS neurons. *J Neurosci* **15**, 4298-4314 (1995).
26. Oliver, K.L., Franceschetti, S., Milligan, C.J., Muona, M., Mandelstam, S.A., Canafoglia, L., *et al.* Myoclonus epilepsy and ataxia due to KCNC1 mutation: Analysis of 20 cases and K(+) channel properties. *Ann Neurol* **81**, 677-689 (2017).
27. Cameron, J.M., Maljevic, S., Nair, U., Aung, Y.H., Cogné, B., Bézieau, S., *et al.* Encephalopathies with KCNC1 variants: genotype-phenotype-functional correlations. *Ann Clin Transl Neurol* **6**, 1263-1272 (2019).
28. Muona, M., Berkovic, S.F., Dibbens, L.M., Oliver, K.L., Maljevic, S., Bayly, M.A., *et al.* A recurrent de novo mutation in KCNC1 causes progressive myoclonus epilepsy. *Nat Genet* **47**, 39-46 (2015).
29. Li, X., Zheng, Y., Li, S., Nair, U., Sun, C., Zhao, C., *et al.* Kv3.1 channelopathy: a novel loss-of-function variant and the mechanistic basis of its clinical phenotypes. *Ann Transl Med* **9**, 1397 (2021).
30. Park, J., Koko, M., Hedrich, U.B.S., Hermann, A., Cremer, K., Haberlandt, E., *et al.* KCNC1-related disorders: new de novo variants expand the phenotypic spectrum. *Ann Clin Transl Neurol* **6**, 1319-1326 (2019).
31. Xu, M., Cao, R., Xiao, R., Zhu, M.X. & Gu, C. The axon-dendrite targeting of Kv3 (Shaw) channels is determined by a targeting motif that associates with the T1 domain and ankyrin G. *Journal of Neuroscience* **27**, 14158-14170 (2007).
32. Xu, M., Gu, Y., Barry, J. & Gu, C. Kinesin I transports tetramerized Kv3 channels through the axon initial segment via direct binding. *Journal of Neuroscience* **30**, 15987-16001 (2010).
33. Fradley, R.L., O'Meara, G.F., Newman, R.J., Andrieux, A., Job, D. & Reynolds, D.S. STOP knockout and NMDA NR1 hypomorphic mice exhibit deficits in sensorimotor gating. *Behav Brain Res* **163**, 257-264 (2005).
34. Parekh, P.K., Sidor, M.M., Gillman, A., Becker-Krail, D., Bettelini, L., Arban, R., *et al.* Antimanic Efficacy of a Novel Kv3 Potassium Channel Modulator. *Neuropsychopharmacology* **43**, 435-444 (2018).
35. Tortosa, E., Adolfs, Y., Fukata, M., Pasterkamp, R.J., Kapitein, L.C. & Hoogenraad, C.C. Dynamic Palmitoylation Targets MAP6 to the Axon to Promote Microtubule Stabilization during Neuronal Polarization. *Neuron* **94**, 809-825 e807 (2017).
36. McDonald, A.J. & Mascagni, F. Differential expression of Kv3.1b and Kv3.2 potassium channel subunits in interneurons of the basolateral amygdala. *Neuroscience* **138**, 537-547 (2006).

37. Couegnas, A., Schweitzer, A., Andrieux, A., Ghandour, M.S. & Boehm, N. Expression pattern of STOP lacZ reporter gene in adult and developing mouse brain. *J Neurosci Res* **85**, 1515-1527 (2007).
38. Dotti, C.G., Sullivan, C.A. & Banker, G.A. The establishment of polarity by hippocampal neurons in culture. *J Neurosci* **8**, 1454-1468 (1988).
39. Gu, Y., Jukkola, P., Wang, Q., Esparza, T., Zhao, Y., Brody, D., *et al.* Polarity of varicosity initiation in central neuron mechanosensation. *J Cell Biol* **216**, 2179-2199 (2017).
40. Nestler, E.J., Barrot, M. & Self, D.W. DeltaFosB: a sustained molecular switch for addiction. *Proc Natl Acad Sci U S A* **98**, 11042-11046 (2001).
41. Barry, J., Gu, Y., Jukkola, P., O'Neill, B., Gu, H., Mohler, P.J., *et al.* Ankyrin-G directly binds to Kinesin-1 to transport voltage-gated Na⁺ channels into axons. *Developmental Cell* **28**, 117-131 (2014).
42. Gu, C. & Barry, J. Function and mechanism of axonal targeting of voltage-sensitive potassium channels. *Prog Neurobiol* **94**, 115-132 (2011).
43. Tweedy, C., Kindred, N., Curry, J., Williams, C., Taylor, J.P., Atkinson, P., *et al.* Hippocampal network hyperexcitability in young transgenic mice expressing human mutant alpha-synuclein. *Neurobiol Dis* **149**, 105226 (2021).
44. Maurer, A.P., Johnson, S.A., Hernandez, A.R., Reasor, J., Cossio, D.M., Fertal, K.E., *et al.* Age-related Changes in Lateral Entorhinal and CA3 Neuron Allocation Predict Poor Performance on Object Discrimination. *Front Syst Neurosci* **11**, 49 (2017).
45. Reagh, Z.M., Noche, J.A., Tustison, N.J., Delisle, D., Murray, E.A. & Yassa, M.A.. Functional Imbalance of Anterolateral Entorhinal Cortex and Hippocampal Dentate/CA3 Underlies Age-Related Object Pattern Separation Deficits. *Neuron* **97**, 1187-1198 e1184 (2018).
46. Babaev, O., Piletti Chatain, C. & Krueger-Burg, D. Inhibition in the amygdala anxiety circuitry. *Exp Mol Med* **50**, 1-16 (2018).
47. Han, S., Tai, C., Westenbroek, R.E., Yu, F.H., Cheah, C.S., Potter, G.B., *et al.* Autistic-like behaviour in Scn1a^{+/-} mice and rescue by enhanced GABA-mediated neurotransmission. *Nature* **489**, 385-390 (2012).
48. Jukkola, P., Gu, Y., Lovett-Racke, A.E. & Gu, C. Suppression of Inflammatory Demyelination and Axon Degeneration through Inhibiting Kv3 Channels. *Front Mol Neurosci* **10**, 344 (2017).
49. Rice, J., Weiner, J.L., Coutellier, L. & Gu, C. Region-Specific Interneuron Demyelination and Heightened Anxiety Induced by Adolescent Binge Alcohol Treatment. *Acta Neuropathologica Communications* **7**, 173 (2019).
50. Jukkola, P., Guerrero, T., Gray, V. & Gu, C. Astrocytes differentially respond to inflammatory autoimmune insults and imbalances of neural activity. *Acta Neuropathologica Communications* **1**, 70 (2013).

51. Sun, C., Qi, L., Cheng, Y., Zhao, Y. & Gu, C. Immediate induction of varicosities by transverse compression but not uniaxial stretch in axon mechanosensation. *Acta Neuropathol Commun* **10**, 7 (2022).
52. Gu, C., Zhou, W., Puthenveedu, M.A., Xu, M., Jan, Y.N. & Jan, L.Y. The microtubule plus-end tracking protein EB1 is required for Kv1 voltage-gated K⁺ channel axonal targeting. *Neuron* **52**, 803-816 (2006).

Acknowledgements

We thank Drs. Howard Gu for technical assistance in stereotaxic injection, David Arnold for technical assistance in rotarod, Laurence Coutellier for consultation in behavioral testing, and OSU Neuroscience Image Core (P30NS104177) for technical assistance in confocal microscopy. This work was supported, in part, by grants from NIH (R01NS093073) to CG. All animal experiments have been conducted in accordance with the NIH Animal Use Guidelines. The authors declare no competing financial interests.

Author contributions

C.G. designed and supervised the research; D.M., S.C., J.B., R.M., H.L., and C.G. performed experiments and made the figures; T.G. and T.M. performed the SPR experiment. C.B. and A.A. provided critical reagents and revised the manuscript. D.M. and C.G. wrote and revised the manuscript.

Competing Interests statement

The authors declare no competing interests.

Figure Legends

Fig. 1: Behavioral alterations in MAP6^{-/-} and Kv3.1^{-/-} mice.

Adult (3-6 months old) WT B6 (black bars), MAP6^{-/-} (red bars), and Kv3.1^{-/-} (green bars) mice were used in a series of behavioral assays. Each group contained approximately half male and half female mice. **a** Example traces in the elevated plus maze (EPM) with open arms indicated in red and closed arms in dark blue. **b** Summaries of open arm time ($100 \times T_{\text{Open}} / (T_{\text{Open}} + T_{\text{Closed}})$); WT control, MAP6^{-/-} $p = 0.001$, Kv3.1^{-/-} $p = 0.029$) (left) and total travel distance (cm; WT control, MAP6^{-/-} $p = 0.088$, Kv3.1^{-/-} $p = 0.003$)(right) in EPM. **c** Example traces in the open field test with blue dashed lines to indicate the center. **d** Summaries of the center time percentage ($100 \times T_{\text{Center}} / T_{\text{Total}}$; Overall $p = 0.595$)(left) and the total travel distance (cm; WT control, MAP6^{-/-} $p = 0.045$, Kv3.1^{-/-} $p = 0.002$)(right) in the open field test. **e** Example traces in the novel object recognition (NOR) test with the blue triangles as the familiar objects (f) and the red circles as the novel objects (n). **f** Summary of the discrimination ratio, $(T_n - T_f) / (T_n + T_f)$. WT control, MAP6^{-/-} $p = 0.044$, Kv3.1^{-/-} $p = 0.096$. **g** Summary of the rotarod test. In trial #3, MAP6^{-/-} $p = 0.041$. In trial #4, MAP6^{-/-} $p = 0.001$. **h** Summary of the balance beam test. **i** Summary of spontaneous alternation in the Y maze test (overall $p = 0.801$). Each result is provided as mean \pm SEM. Mouse numbers are provided in the figure. One-Way ANOVA followed by Dunnett's test: *, $p < 0.05$; **, $p < 0.01$.

Fig. 2: MAP6 deletion markedly reduces Kv3.1b channel level in PV+ GABAergic interneurons.

a A diagram of the coronal section (Bregma -1.82 mm) of mouse brain with boxes (in green) indicating the hippocampal (Hip) and amygdala (AMG) regions. **b** MAP6 and Kv3.1b proteins colocalized in WFA+ cells in the hippocampal CA1 region. In CMYK images with white background, anti-MAP6, anti-Kv3.1b, WFA, and Hoechst staining signals are in cyan, black, magenta, and yellow, respectively. In gray scale images, signals are inverted. **c** MAP6 and Kv3.1b proteins colocalized in GABAergic interneurons of basolateral amygdala. **d** Summary of the percentage of cell bodies with colocalizing MAP6 and Kv3.1b proteins in three different brain regions, Hip, AMG, and substantia nigra (SN). In each group, 10 images from 3 WT mice were included. **e** Confocal images of a MAP6+ and Kv3.1b+ GABAergic interneuron in the hippocampus of a WT mouse. **f** Confocal images of a WFA+ GABAergic interneuron in the

hippocampus of a MAP6^{-/-} mouse. **g** Colocalization of Kv3.1b and PV along an axon segment in WT hippocampus. **h** The absence of Kv3.1b in PV+ axons in MAP6^{-/-} hippocampus. **i** Western blotting of brain lysates from WT, MAP6^{+/-}, MAP6^{-/-} and Kv3.1^{-/-} mice with anti-MAP6 (top), anti-Kv3.1b (middle) or anti- β -tubulin (bottom as an input control) antibody. Molecular weights are on the left in kDa. **j** Summaries of Western blotting results (mean \pm SEM) using the anti-Kv3.1b (Left; Unpaired t-test: $p = 0.001$) or anti-MAP6 antibody (Right; One-Way ANOVA followed by Dunnett's test: MAP6^{-/-} $p = 0.001$, Kv3.1^{-/-} $p = 0.552$). The mouse number of each group is provided within the bar. ** $p < 0.01$. Scale bars in white, 200 μ m in **(b)** and **(c)**, and 25 μ m in **(e)-(h)**.

Fig. 3: MAP6 directly binds Kv3.1 channel N-terminus.

a Tissue co-IP experiment. Mouse brain lysates were pulled down by an anti-Kv3.1b antibody, mouse IgG (mIgG as the negative control), or an anti-MAP6 antibody (10% loaded as the positive control), and resolved in Western blotting with the anti-MAP6 antibody. **b** The diagram of Kv3.1b structure and GST-fusion proteins. **c** Purified GST-fused Kv3.1 T1 domain (GST-31T1) but not C-terminus (GST-31aC), nor Kv1.2 cytoplasmic domains (GST-12N and GST-12C), pulled down MAP6N-GFP (anti-GFP Western, top) expressed in HEK293 cells. Inputs of GST fusion proteins are shown with Colloidal blue staining (bottom). **d** Structural diagrams of the full-length MAP6N and its truncations. Mn modules: red bars. Mc modules: the gray bar. The C terminal domain: the open bar. **e-g** Purified GST-31T1 pulled down MAP6N-GFP, MAP6E-GFP, Δ Mc-GFP, Δ PPP-GFP, His-MAP61, and His-MAP62, but not His-MAP63 and His-MAP64. **h** Structural diagrams of MAP62 and its fragments. **i** Purified GST-M115-221 and GST-M115-184 (the two Mn modules) but not others pulled down bacterially-expressed His-31T1. Numbers on the left: molecular weight in kDa.

Fig. 4: Two MAP6 Mn modules bind both monomers and tetramers of Kv3.1 T1 domain.

a Structural diagrams of Kv3.1 tetramer, MAP6N, and KIF5 dimer. **b** Purified GST-M115-221 but not GST-KIF5BTail pulled down His-31T1 in the absence and presence of 1 mM EDTA. **c** Each Zn²⁺ binding site involves 1 His and 3 Cys residues from two adjacent T1 domains in the tetramer. **d** An enlarged view

of a Zn^{2+} -binding site formed by C83 from the purple T1 domain and H77/C104 from the green T1 domain. **e** Purified GST-M115-221 and GST-M115-184 pulled down His-31T1 and His-C83A (C83 to Ala), but not His-H77A (H77 to Ala) and His-C2A2 (C104 and C105 to two Alas). The anti-His Western is on the top and Colloidal blue staining for the inputs is at the bottom. **f** Purified GST-M115-221 pulled down purified His-31T1. The black arrow, protein bands for His-31T1. **g** Binding traces in the SPR experiment. Five different concentrations (in different colors) of purified GST-M115-221 sequentially flowed over the His-31T1-coated surface.

Fig. 5: MAP6 binding regulates the protein levels of Kv3.1b channels in the soma and axonal terminals of primary cultured neurons.

Cultured hippocampal neurons were co-transfected with Kv3.1b and MAP6 constructs at 6 days *in vitro* (DIV) and fixed for immunostaining 2-3 days later. **a** Kv3.1bHA, and MAP6-GFP were highly colocalized. Signals were inverted in gray scale images. **b** Confocal images showed high colocalization between Kv3.1bHA (red in the merged) and MAP6N-GFP (green in the merged) in the cell body (top) and axonal terminals (bottom). **c** Kv3.1bHA_{H77} was restricted in the soma, whereas MAP6N-GFP was present throughout the axons. **d** Confocal images showed low levels of Kv3.1bHA_{H77} and MAP6N-GFP in the soma (top), and the absence of Kv3.1bHA_{H77} and a high level of MAP6N-GFP in distal axons (bottom). **e** Both Kv3.1bHA_{KKK} and MAP6N-GFP were restricted in the soma. **f** Confocal images showed high colocalization of the two in the soma. **g** Both Kv3.1bHA and MAP6NΔ1-GFP were restricted in the soma. **h** Confocal images showed high colocalization of the two in the soma. Scale bars, 100 μm in (a), (c), (e), (g), and 25 μm in (b), (d), (f), (h). **i** Summary of the ratio of HA staining intensities between the axon and soma under the 4 conditions. One-Way ANOVA followed by Dunnett's test: Kv3.1b-HA+MAP6N-GFP control, n = 14; Kv3.1b-HA_{H77}+MAP6N-GFP $p = 0.001$, n = 13; Kv3.1b-HA_{KKK}+MAP6N-GFP $p = 0.001$, n = 10; Kv3.1b-HA+MAP6NΔ1-GFP $p = 0.003$, n = 19. **j** Summary of the ratio of GFP fluorescence intensities between the axon and soma (for the 4 conditions: control; $p = 0.003$; $p = 0.031$; $p = 0.008$). **k** Summary of HA staining intensities in the soma (for the 4 conditions: control; $p = 0.002$; $p = 0.009$; $p = 0.015$). One-Way ANOVA followed by Dunnett's test: *, $p < 0.05$; **, $p < 0.01$.

Fig. 6: AAV-mediated knockdown of MAP6 in the amygdala reduced risk avoidance in mice and Kv3.1b channel level in infected neurons.

a Diagram of AAV stereotaxic injection in the amygdala (top) and an example of coronal section of injected mouse brain expressing GFP (bottom, signals are inverted). **b** EPM traces of mice injected with AAV expressing control shRNA or MAP6 shRNA. Closed arms are indicated in dark blue and open arms in red. **c** Summaries of open-arm-time percentage (Left; Unpaired t-test: $p = 0.018$) and total travel distance (Right; $p = 0.611$). **d** Example open-field traces of mice injected with AAV expressing control shRNA or MAP6 shRNA. The center region is indicated with a blue dashed box. **e** Summaries of the percentage of center time (Left, $p = 0.0431$) and total travel distance (Right; $p = 0.564$). **f-i** Comparisons of rotarod, balance beam, Y maze, and NOR results from the mice injected with AAV expressing either control shRNA (black) or MAP6 shRNA (red). **j** Basolateral amygdala neurons infected by AAV expressing control shRNA (indicated by GFP (cyan in the merged) were stained for endogenous MAP6 (magenta in the merged) and Kv3.1b (black in the merged). Hoechst stain is in yellow in the merged. Signals are inverted in gray scale images. **k** Basolateral amygdala neurons infected by AAV expressing MAP6 shRNA. **l** Confocal CMYK images of stained neurons expressing control shRNA (top) or MAP6 shRNA (bottom). White asterisk in the lower panel: an uninfected neuron (no GFP expression) expressing MAP6 (magenta) and Kv3.1b (black). Scale bars, 300 μm in (**j**) and (**k**), and 25 μm in (**l**). **m** Summary of the percentage of GFP+ cells expressing MAP6 (Left; control shRNA $n = 1367$, MAP6 shRNA $n = 909$) or Kv3.1b (Right) from the amygdala. Unpaired t-test: *, $p < 0.05$; **, $p < 0.01$; ***, $p < 0.001$.

Fig. 7: Deleting MAP6 in the hippocampus induced hyperactivity and memory deficits in mice, and increased the activity of hippocampal CA3 pyramidal neurons.

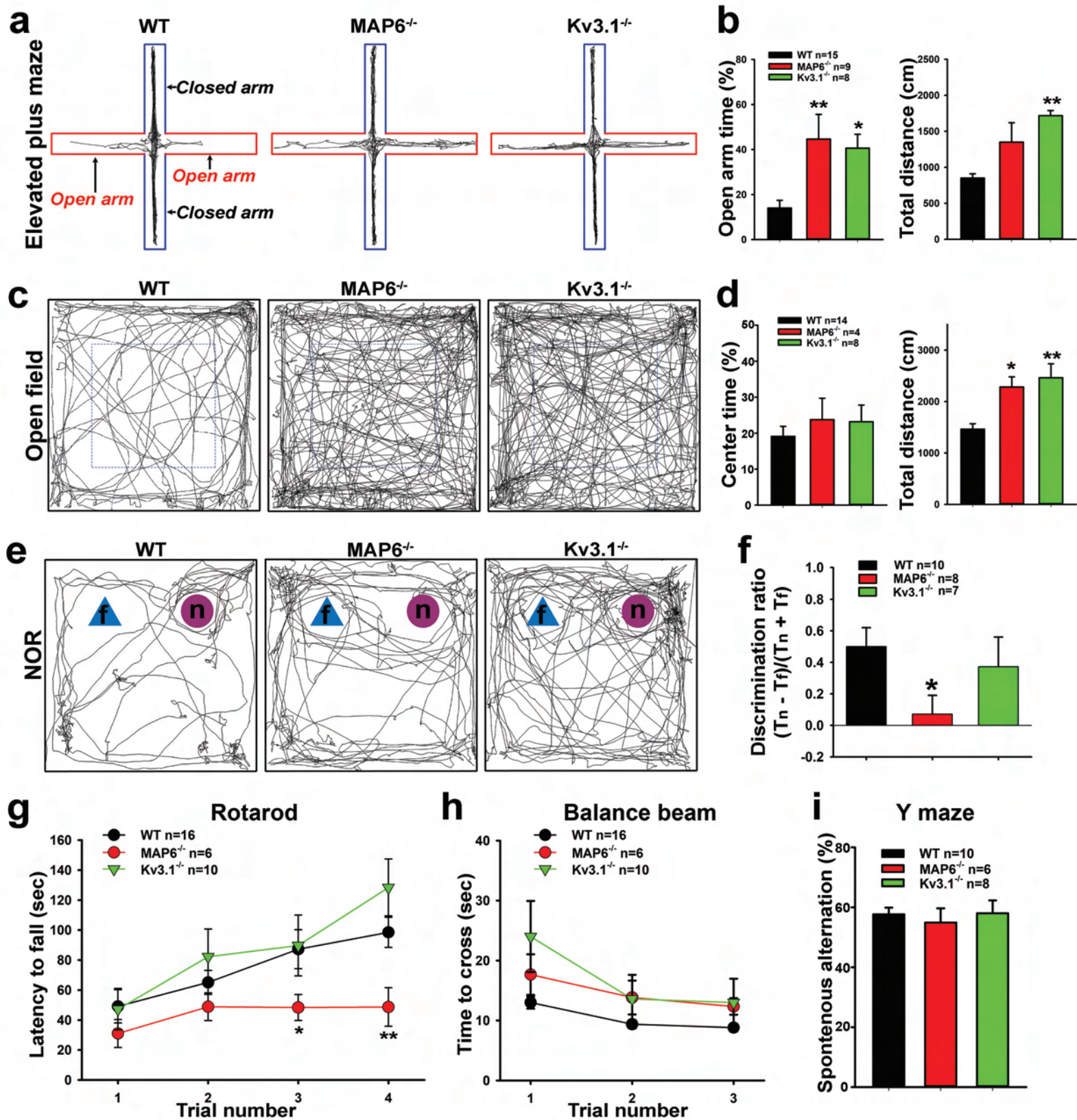
a Diagram of AAV stereotaxic injection in the hippocampus (top) and an example of coronal section of injected mouse brain expressing GFP (bottom, signals are inverted). **b** NOR traces of mice injected with AAV expressing control shRNA or MAP6 shRNA. **c** The summary of discrimination ratio in the NOR

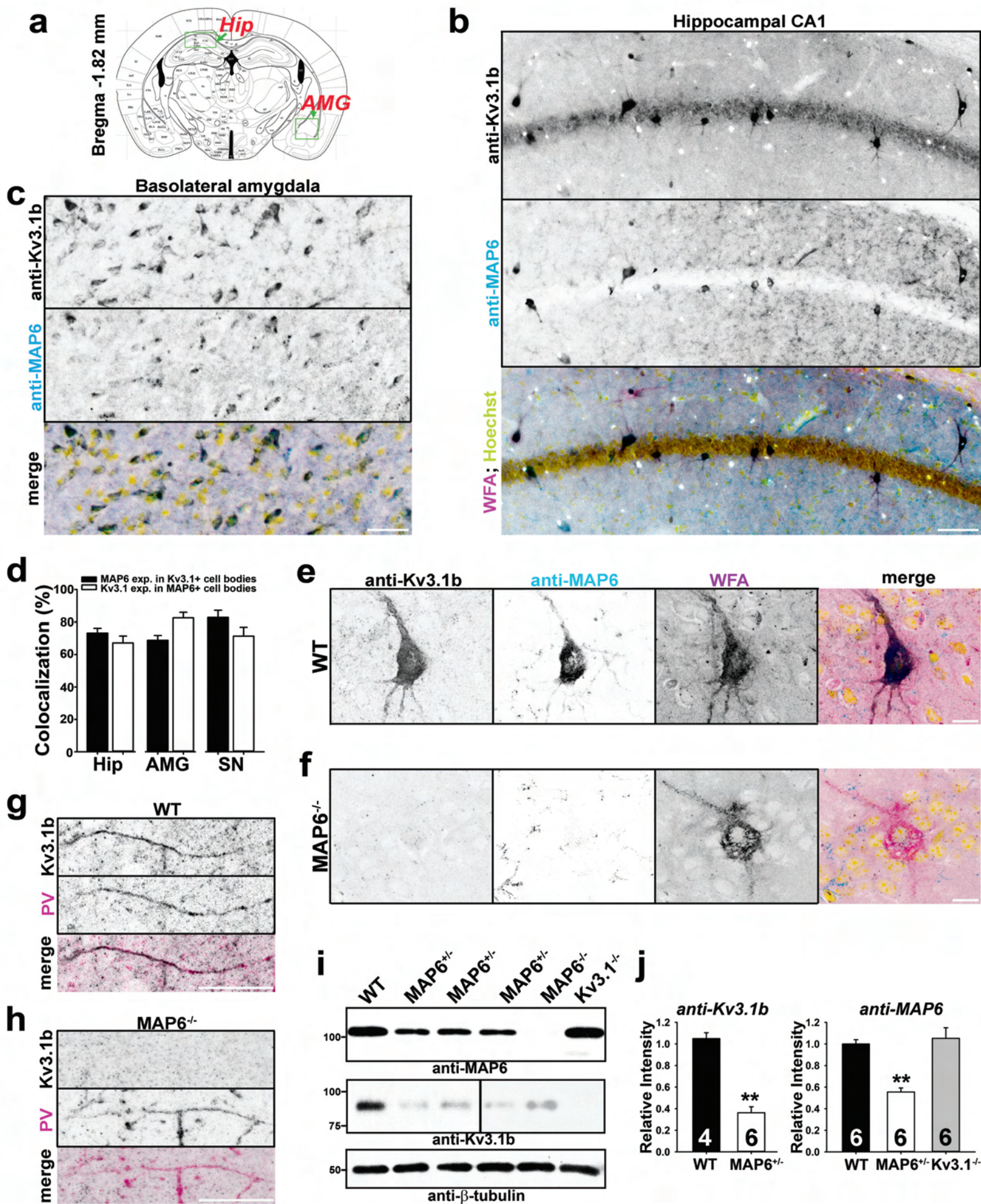
assay (Unpaired t-test, $p = 0.0434$) **d-h** Comparisons of open field, EPM, rotarod, balance beam, and Y maze results from the mice injected with AAV expressing either control shRNA (black) or MAP6 shRNA (red). **i** CMYK images brain sections for Δ FosB (black), PV (magenta), and Hoechst (yellow) staining and for AAV infection shown by GFP (cyan) in the CA3 region of hippocampus from mice injected with AAV expressing either control shRNA (left) or MAP6 shRNA (right). **j** Summary of the Δ FosB/Hoechst ratio for different conditions. Hip CA3, hippocampal CA3 (Unpaired t-test: $p = 0.0001$; control shRNA $n = 4241$, MAP6 shRNA $n = 5054$). AMG BLA, basolateral amygdala (Unpaired t-test: $p = 0.0001$; control shRNA $n = 6583$, MAP6 shRNA $n = 6741$). **k** Confocal CMYK image of a neuron infected by AAV containing control shRNA in CA3. **l** Confocal CMYK image of a neuron infected by AAV containing control shRNA in CA3. Scale bars, 300 μ m in (**i**) and 25 μ m in (**k**) and (**l**). Unpaired t-test: *, $p < 0.05$; ***, $p < 0.001$.

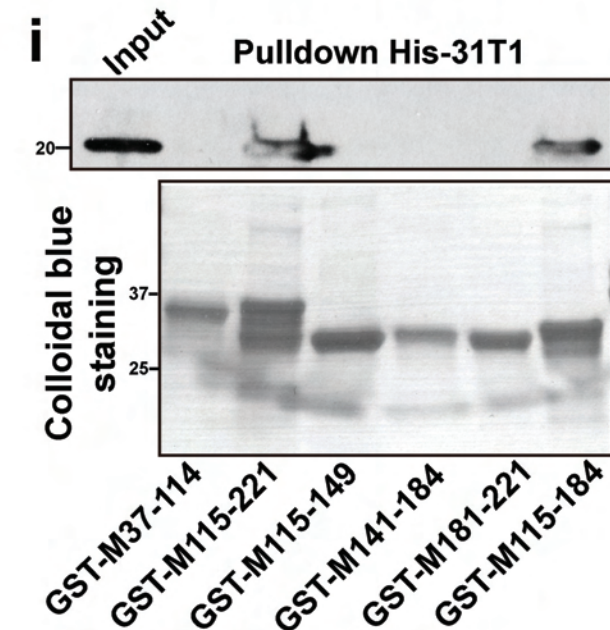
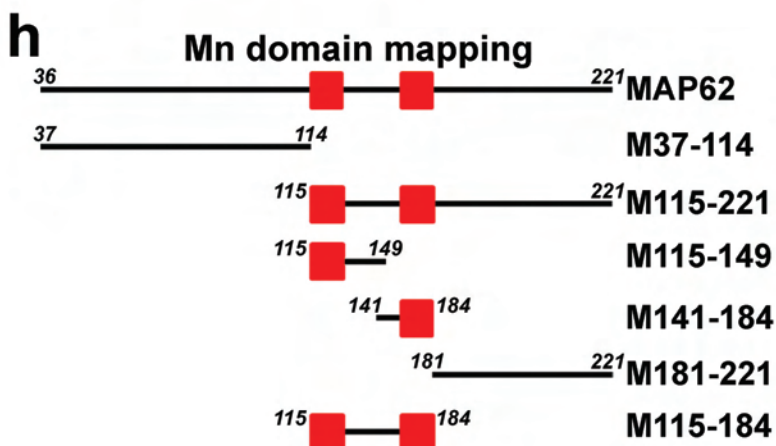
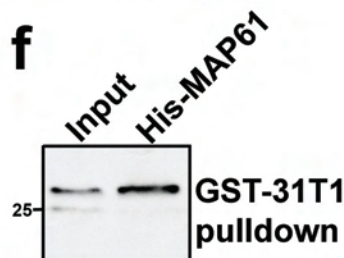
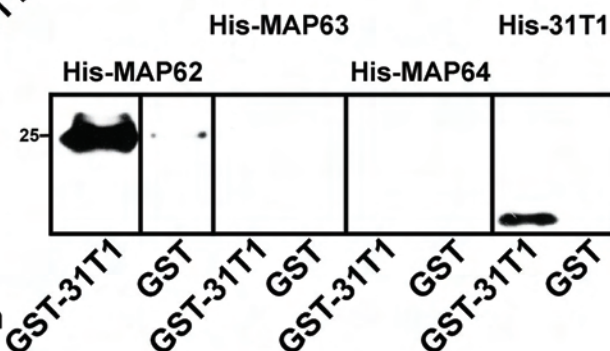
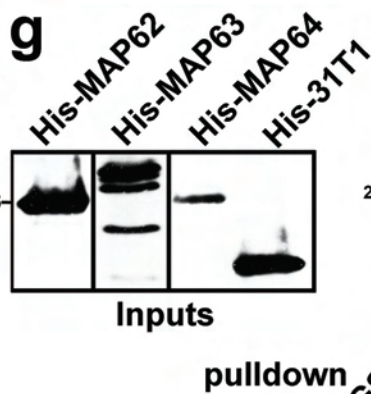
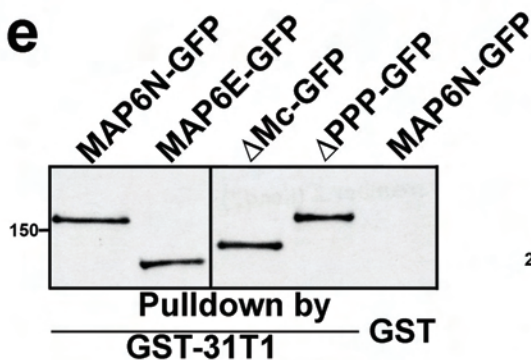
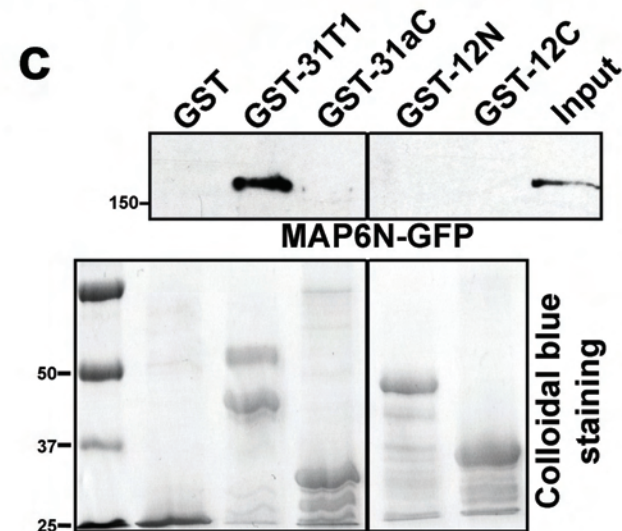
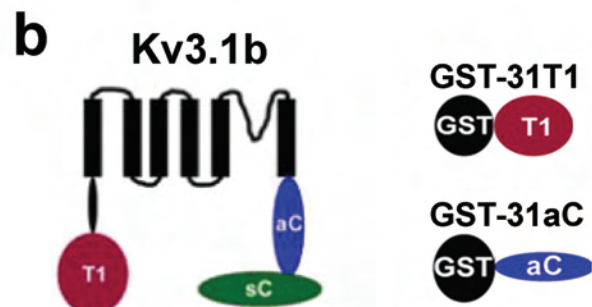
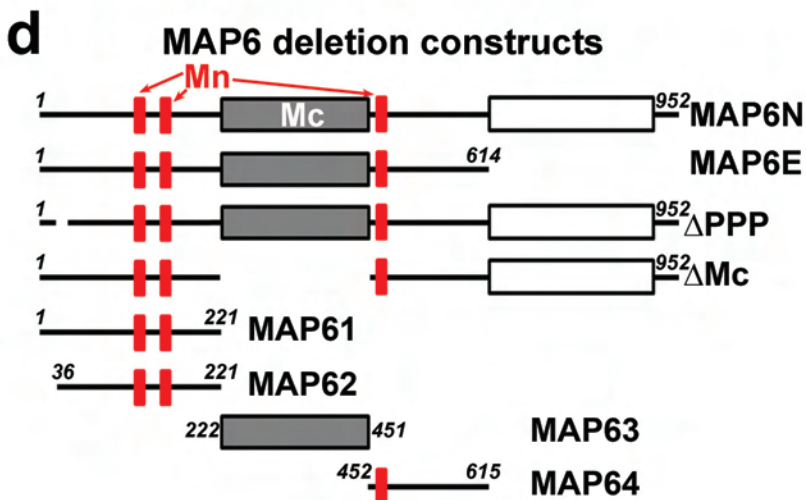
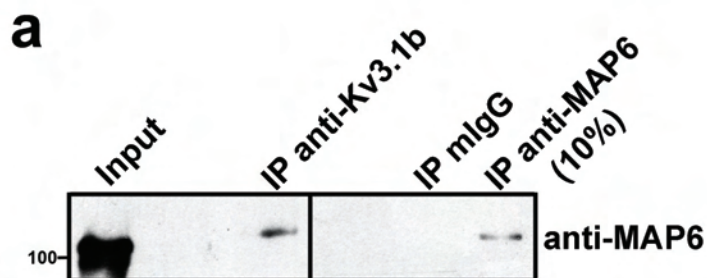
Fig. 8: Kv3.1 knockdown in the amygdala or hippocampus reduced risk avoidance and induced hyperactivity.

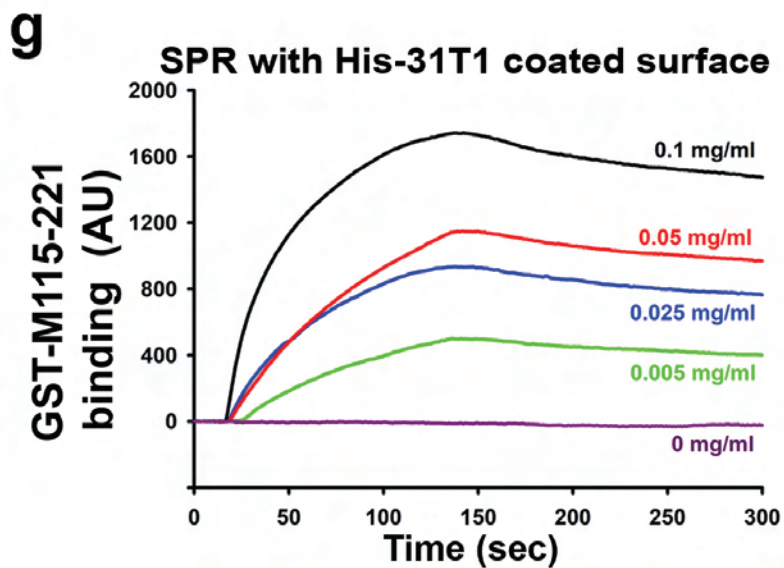
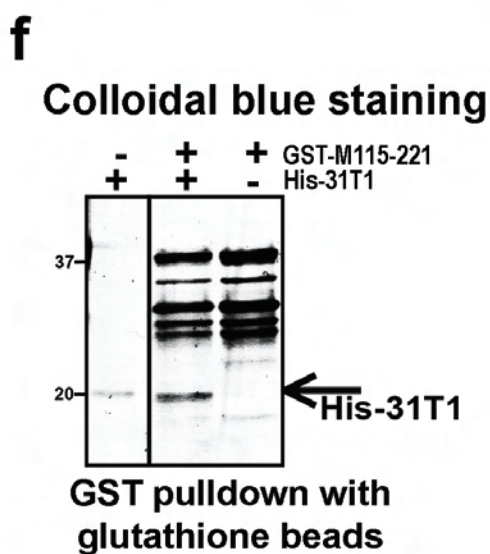
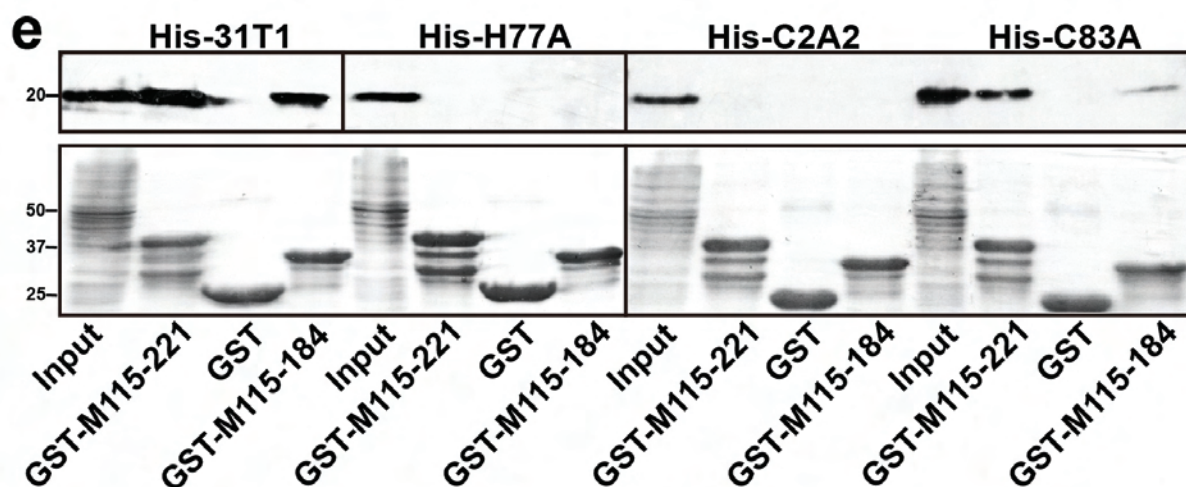
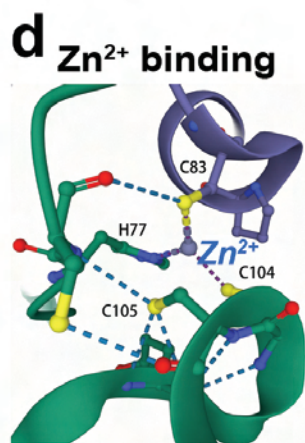
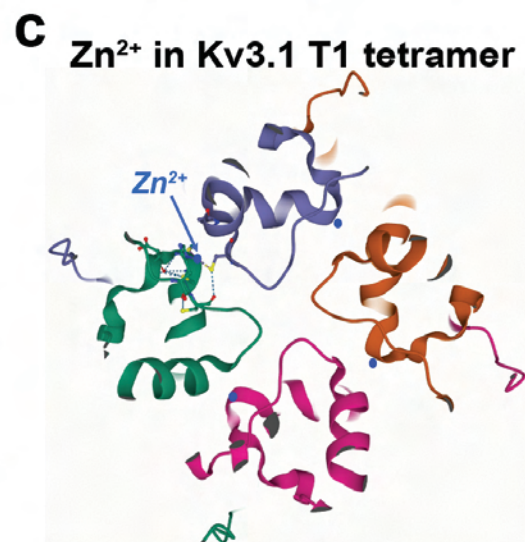
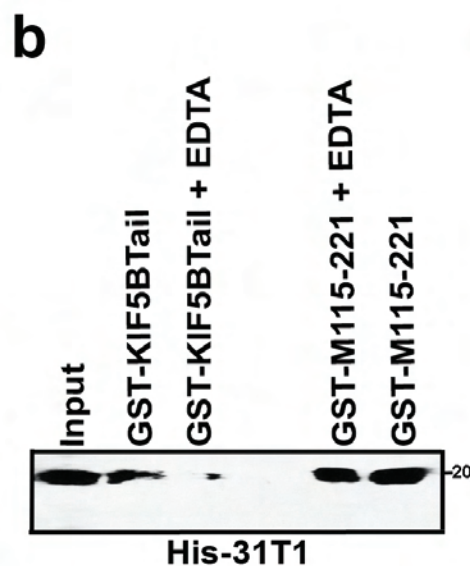
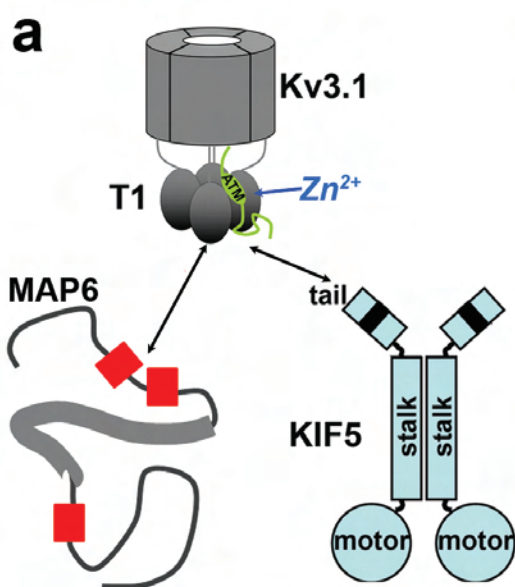
a,b Summaries of open-arm-time percentage (Unpaired t-test, $p = 0.005$) and total travel distance in EPM (top; $p = 0.035$), and center-time percentage ($p = 0.015$) and total travel distance ($p = 0.059$) in OF (open field, bottom)), using mice with the injection of AAV-Kv3.1-shRNA (AAV-control-shRNA as control) in the amygdala. **c,d** Summaries of open-arm-time percentage (Unpaired t-test, $p = 0.012$) and total travel distance ($p = 0.378$) in EPM (top), and center-time percentage ($p = 0.712$) and total travel distance ($p = 0.002$) in OF (open field, bottom), using mice with the injection of AAV-Kv3.1-shRNA (AAV-control-shRNA as control) in the hippocampus. **e** No change in NOR in mice with the AAV injection in either amygdala ($p = 0.813$) or hippocampus ($p = 0.102$) to knock down Kv3.1. **f** The injection of AAV-Kv3.1-shRNA in the amygdala markedly reduced Kv3.1 expression, shown by the injection diagram (left), representative images (middle), and quantification (right) ($p = 0.0001$). In the images, GFP is in cyan, Kv3.1b in black and Hoechst in yellow. For each condition, 18 images were included in the quantification. **g** The injection of AAV-Kv3.1-shRNA in the hippocampal CA3 region markedly reduced Kv3.1 expression ($p = 0.0001$). **h** High magnification confocal image of a PV+/Kv3.1b+ interneuron infected by AAV-control-shRNA in the hippocampus. PV staining is in magenta. **i** High magnification confocal image of a

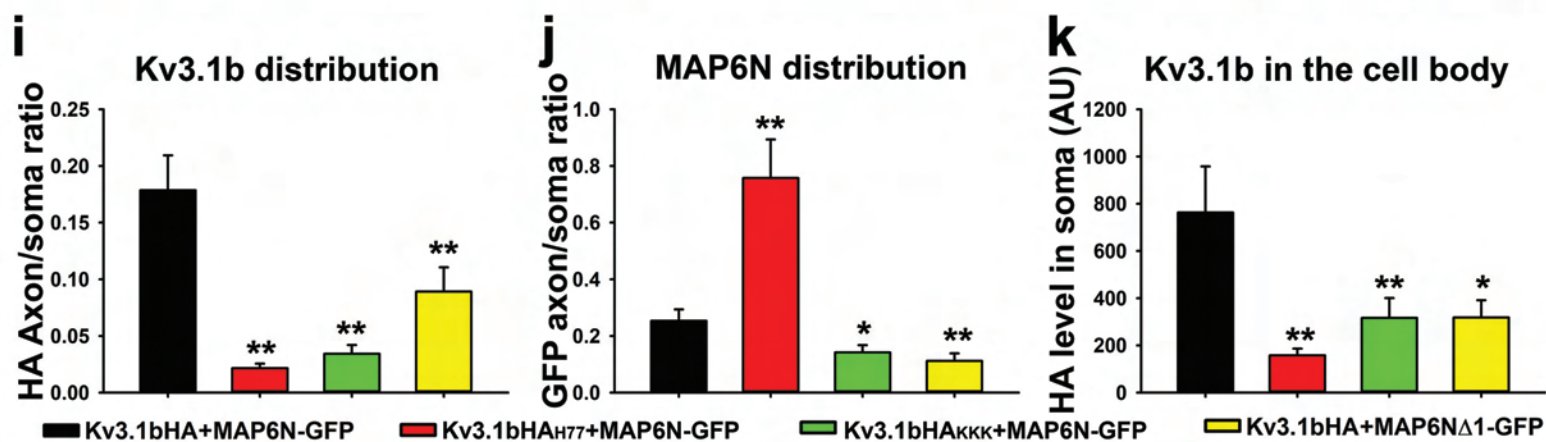
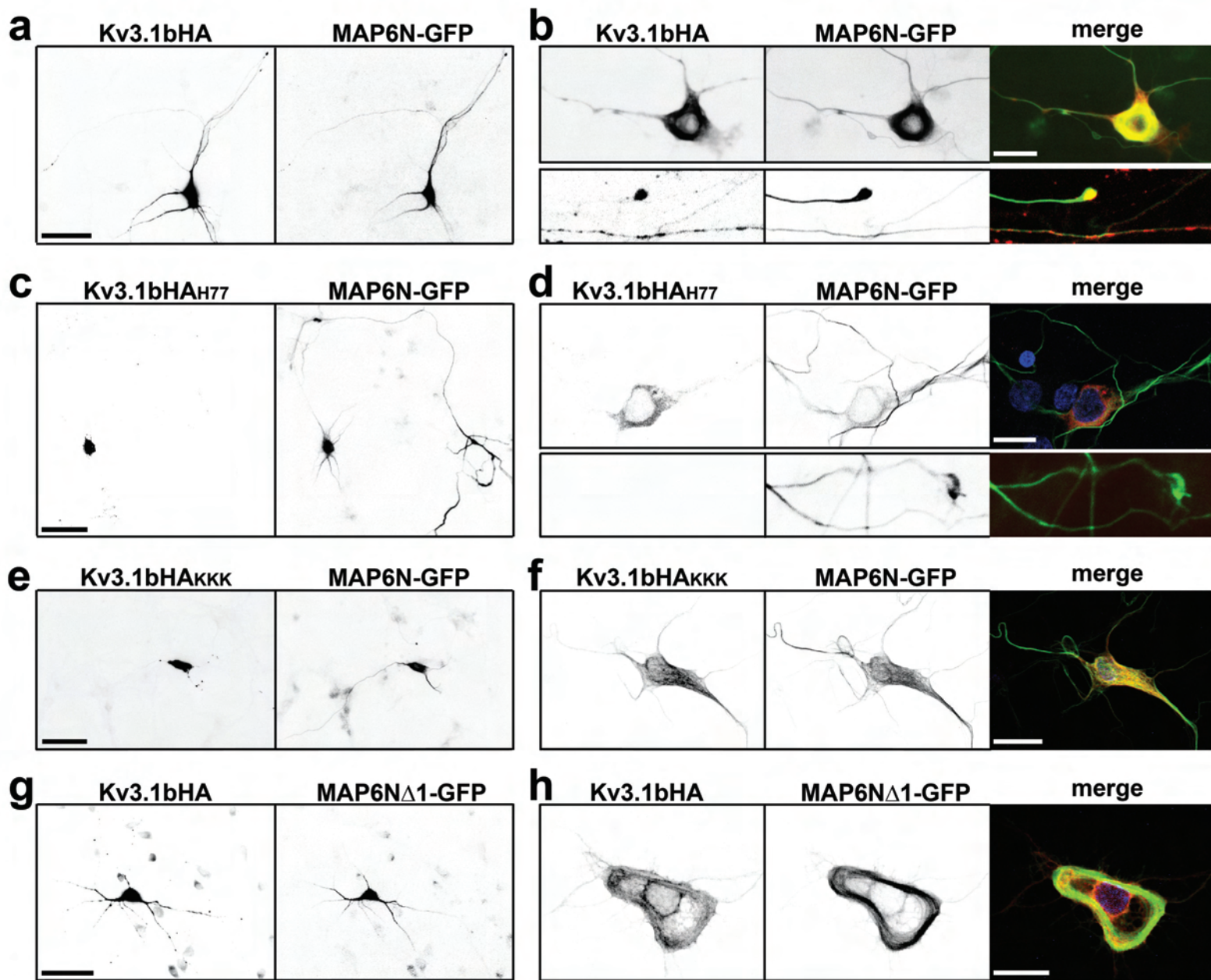
PV+ interneuron infected by AAV-Kv3.1-shRNA with no Kv3.1b staining signal. Scale bars, 300 μm in (f) and (g), and 30 μm in (h) and (i). Unpaired t-test: *, $p < 0.05$; **, $p < 0.01$; ***, $p < 0.001$.

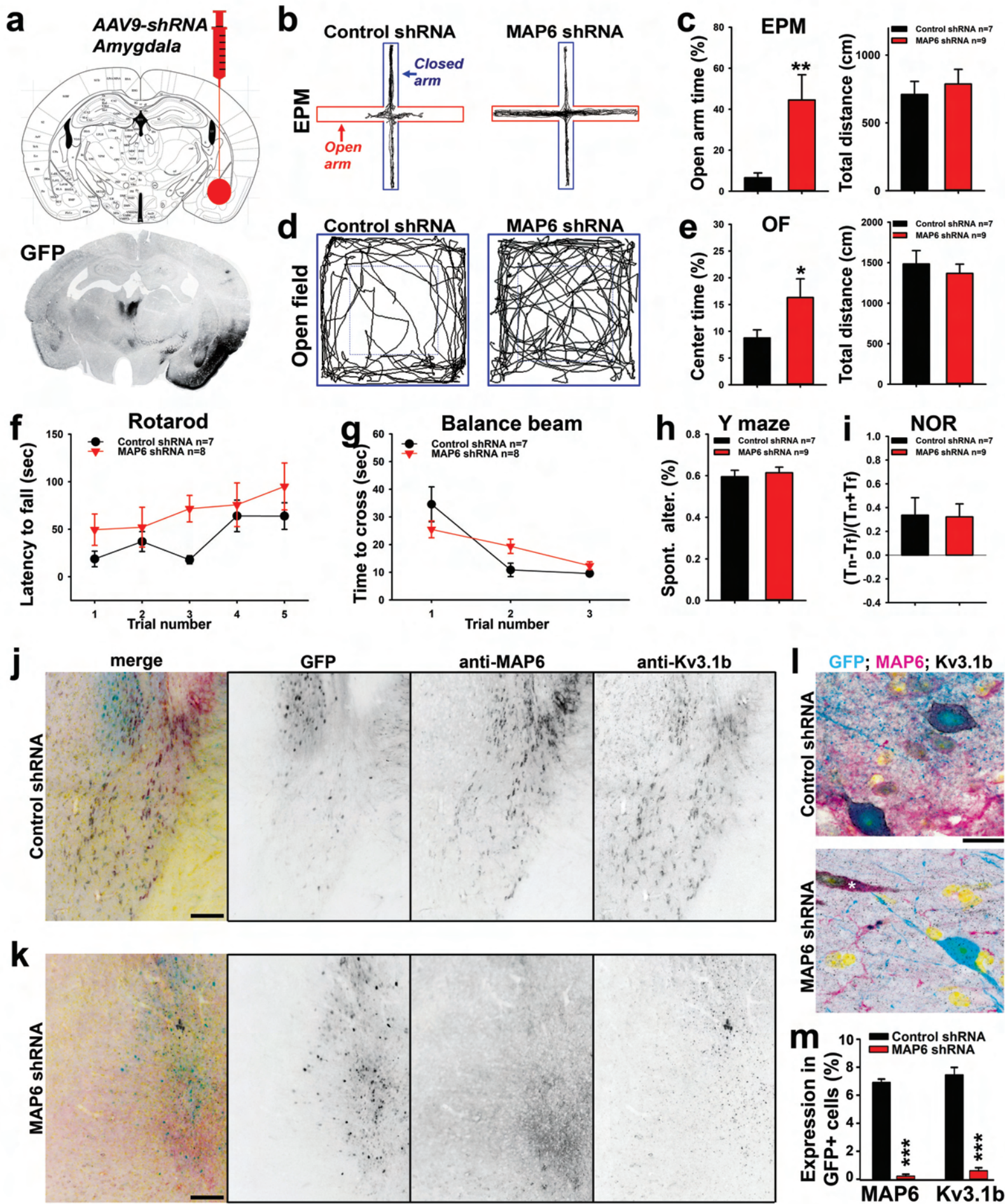


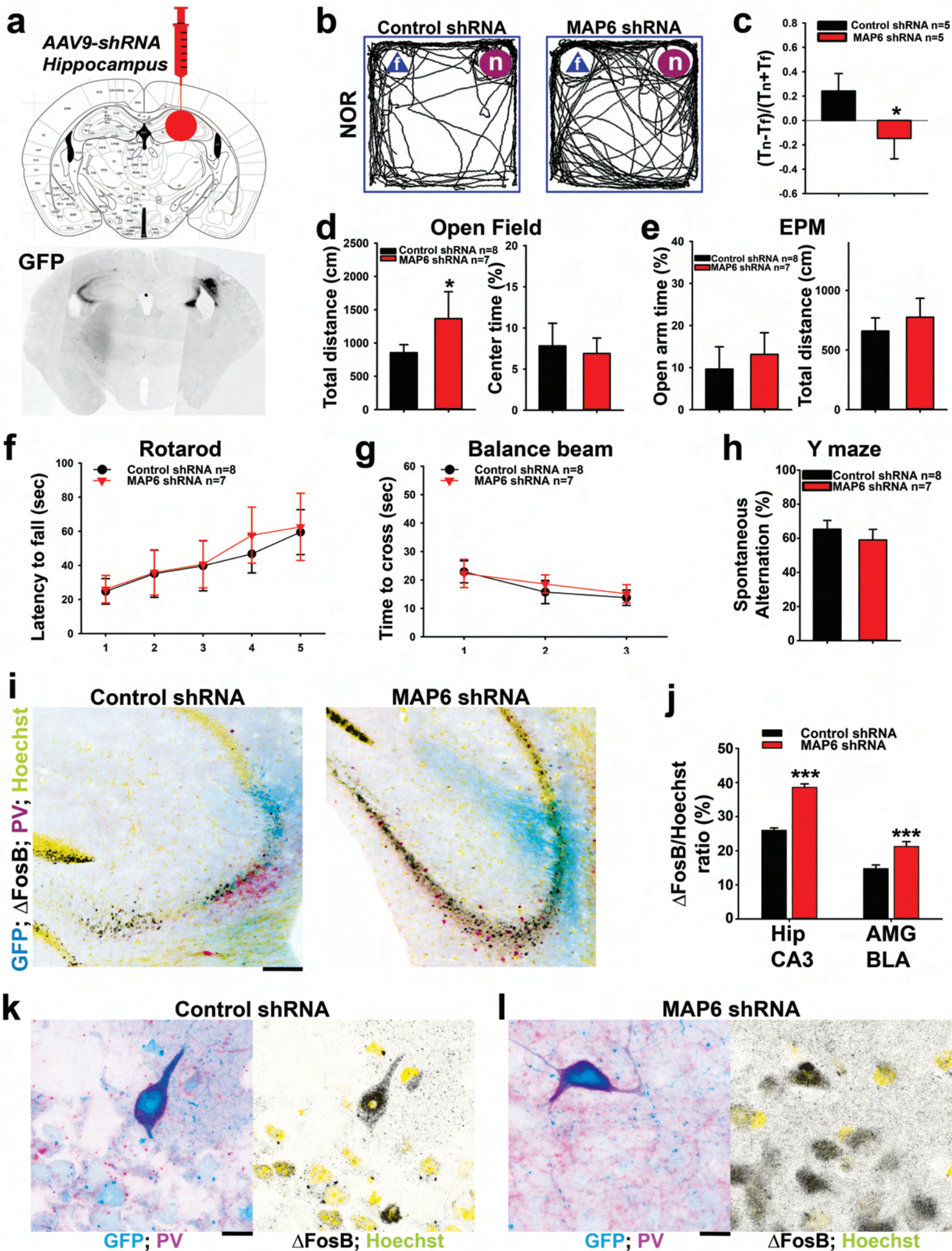


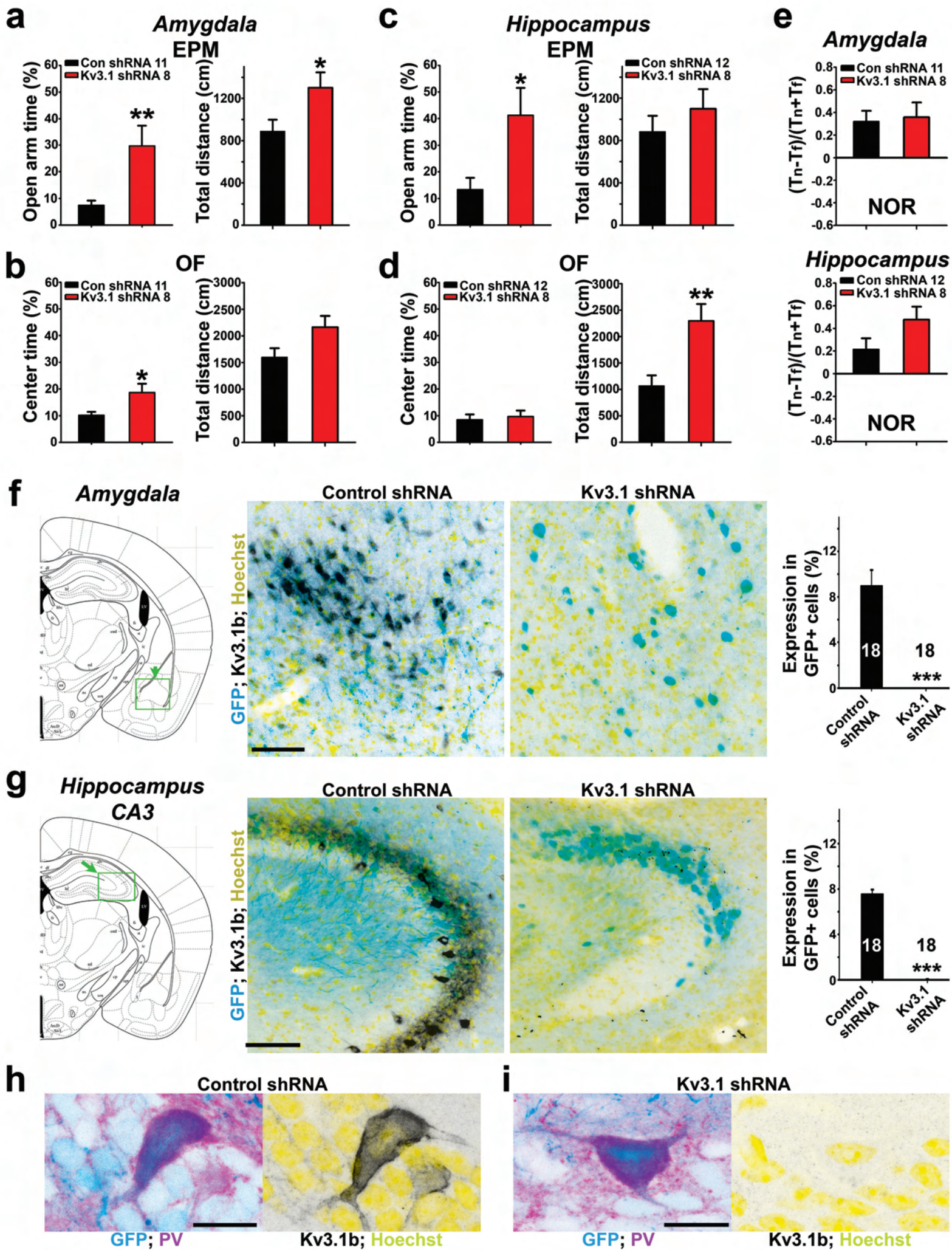






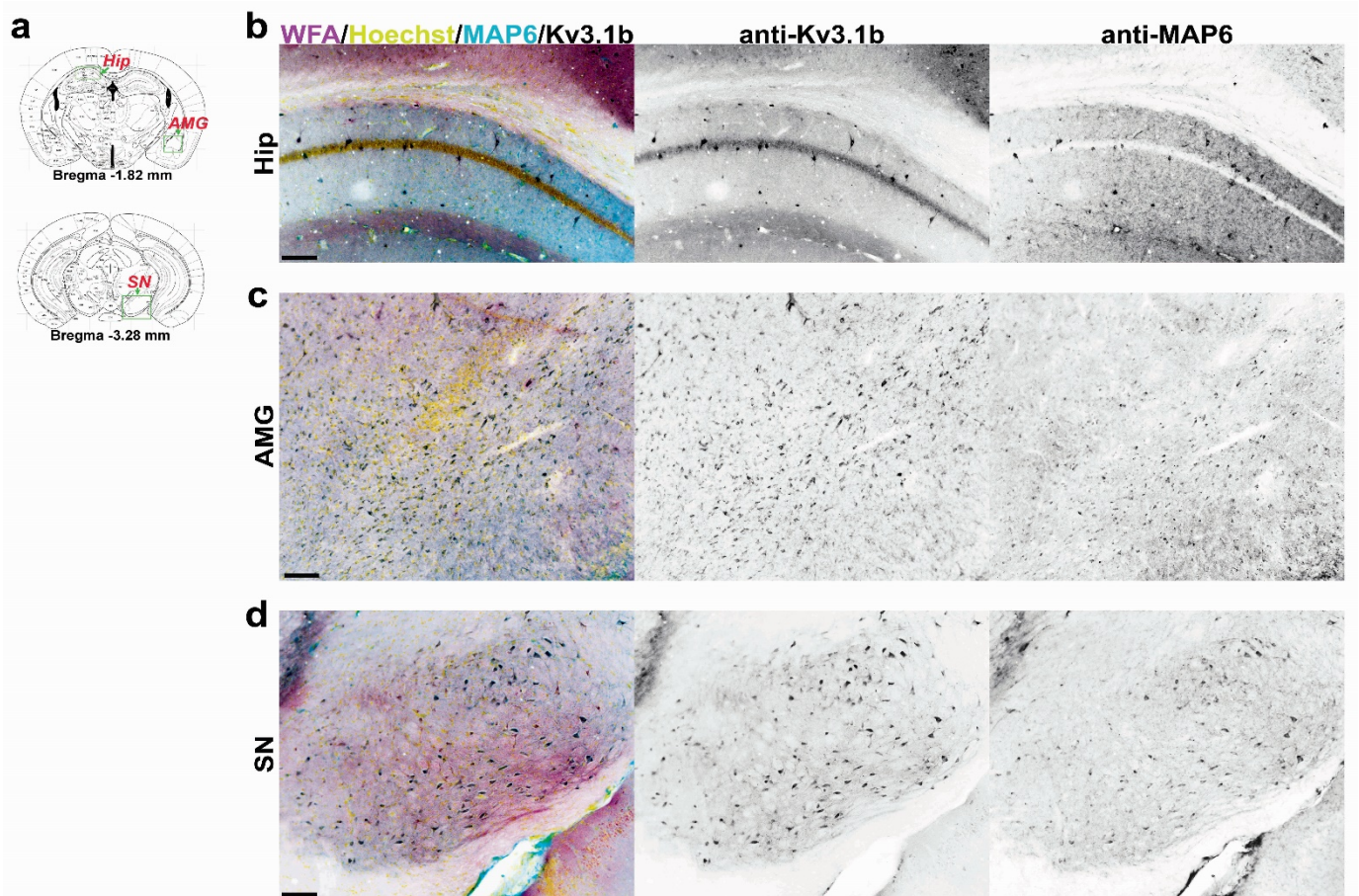






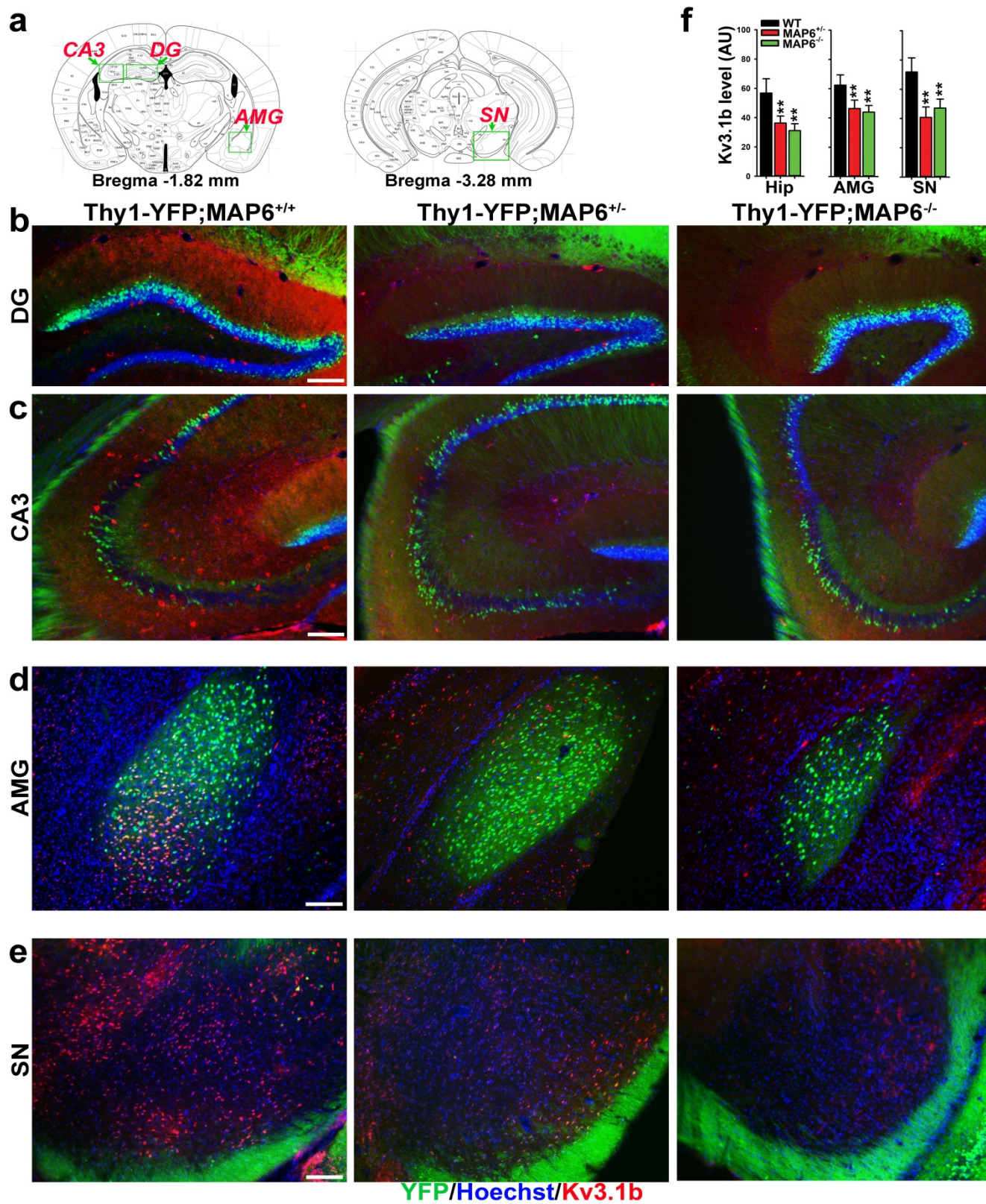
Supplemental Information for
A cytoskeleton-membrane interaction conserved in fast-spiking neurons controls
movement, emotion, and memory

Di Ma^{1,2}, Chao Sun^{2,3}, Rahul Manne², Tianqi Guo⁴, Christophe Bosc⁵, Joshua Barry^{2,§}, Thomas Magliery⁴,
Annie Andrieux⁵, Houzhi Li², and Chen Gu^{1,2,3*}



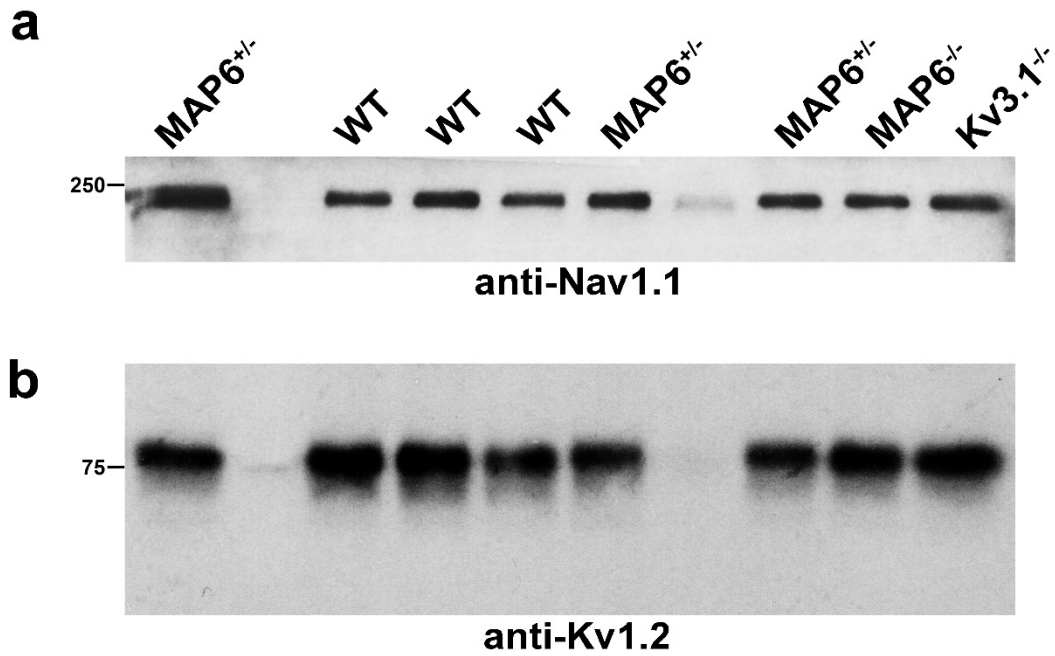
Supplementary Fig. S1: Colocalization of MAP6 and Kv3.1b proteins in WFA+ GABAergic interneurons in different regions of the mouse brain.

a Diagrams of coronal sections of WT mouse brain show the positions (green boxes) for the hippocampus (Hip), amygdala (AMG), and substantia nigra (SN). **b-d** Example images of the three brain regions. In CMYK merged images with white background, the anti-Kv3.1b, anti-MAP6, WFA, and Hoechst staining signals are in black, cyan, magenta, and yellow, respectively. In grayscale images, signals are inverted. Scale bars, 300 μm .



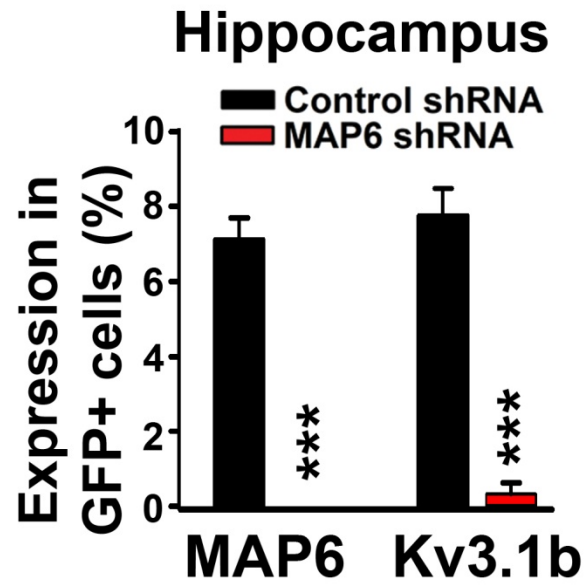
Supplementary Fig. S2: MAP6 deletion markedly reduced Kv3.1b protein levels in GABAergic interneurons in multiple regions of the mouse brain.

a Diagrams of coronal sections of WT mouse brain show the positions (green boxes) for CA3 (hippocampal CA3), DG (hippocampal dentate gyrus), AMG (amygdala), and SN (substantia nigra). MAP6^{+/-} mice were crossed with Thy1-YFP-H transgenic mice to give rise to the WT (Thy1-YFP;MAP6^{+/+}), heterozygous (Thy1-YFP;MAP6^{+/-}) and homozygous (Thy1-YFP;MAP6^{-/-}) mice. **b-e** Example images of the four brain regions. In RGB merged images with white background, the anti-Kv3.1b (red) and Hoechst (blue) staining signals, as well as YFP (green) fluorescence signals, are provided. **f** Levels of Kv3.1b staining intensity in the three brain regions from WT (black), MAP6^{+/-} (red), and MAP6^{-/-} (green) mice. One-Way ANOVA followed by Dunnett's test: **, $p < 0.01$. $n = 20$ images for each condition. Scale bars, 300 μm .



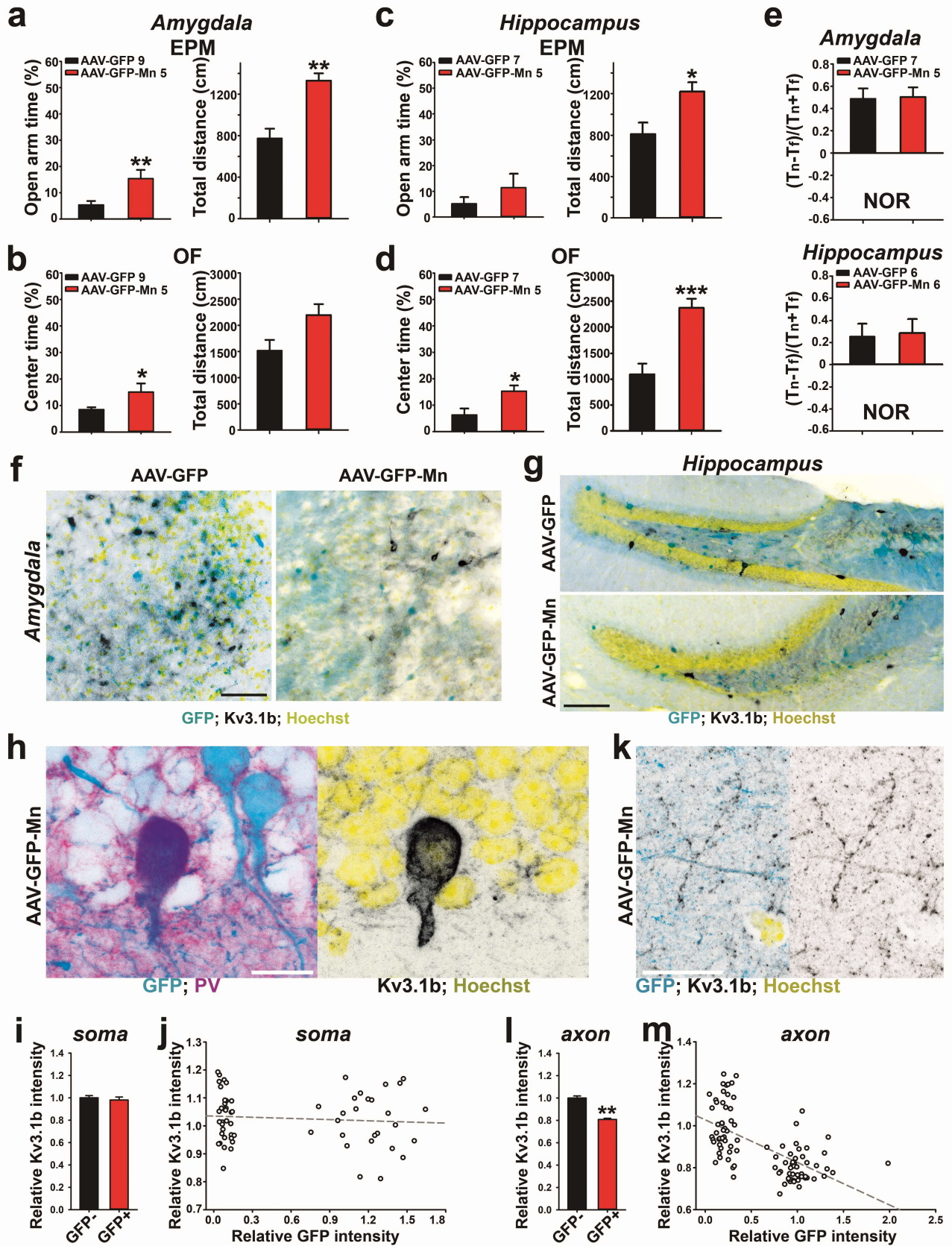
Supplementary Fig. S3: The expression of Nav1.1 and Kv1.2 channel proteins did not change in MAP6 and Kv3.1 KO mice.

Crude membrane lysates of whole brains from WT, MAP6^{+/-}, MAP6^{-/-} and Kv3.1^{-/-} mice were separated with SDS-PAGE and blotted by either a mouse monoclonal anti-Nav1.1 (**a**) or anti-Kv1.2 antibody (**b**). The numbers on the left, molecular weight in kDa.



Supplementary Fig. S4: AAV-MAP6-shRNA markedly reduced the expression of MAP6 and Kv3.1b in infected hippocampal neurons.

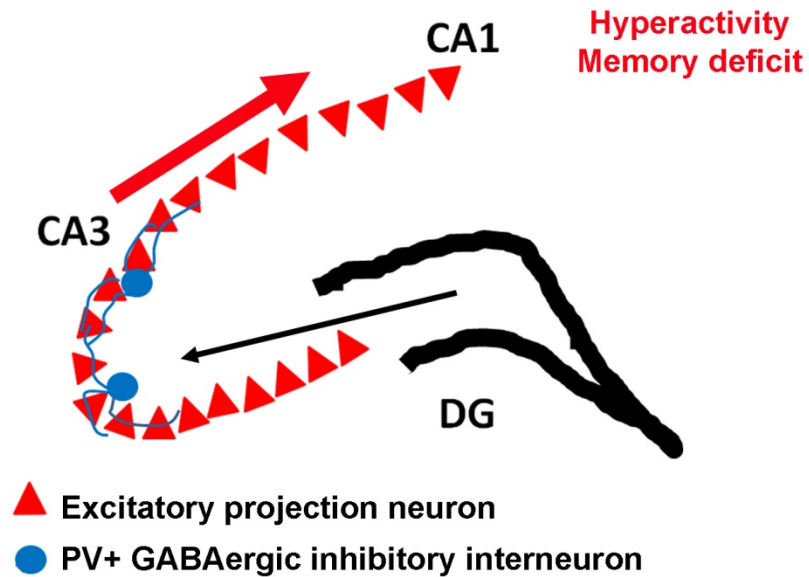
Summary of the percentage of GFP+ cells expressing MAP6 (Left; control shRNA $n = 759$, MAP6 shRNA $n = 322$) or Kv3.1b (Right) from the hippocampus. Unpaired t-test: ***, $p < 0.001$.



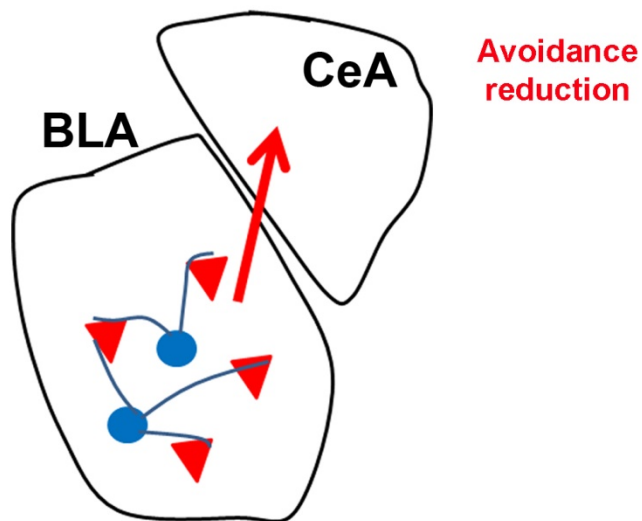
Supplementary Fig. S5: Over-expression of GFP-Mn in the amygdala or hippocampus reduced risk avoidance and induced hyperactivity via reducing Kv3.1b axonal levels.

a,b Summaries of open-arm-time percentage (Left; Unpaired t-test, $p = 0.008$) and total travel distance (Right; $p = 0.002$) in EPM (top), and center-time percentage (Left; $p = 0.026$) and total travel distance (Right; $p = 0.054$) in OF (open field, bottom), using mice with the injection of AAV-GFP-Mn (AAV-GFP as control) in the amygdala. **c,d** Summaries of open-arm-time percentage (Left; $p = 0.267$) and total travel distance (Left; $p = 0.021$) in EPM (top), and center-time percentage (Left; $p = 0.027$) and total travel distance (Right; $p = 0.0001$) in OF (open field, bottom), using mice with the injection of AAV-GFP-Mn (AAV-GFP as control) in the hippocampus. **e** No change in NOR in mice with the AAV injection in either amygdala ($p = 0.904$) or hippocampus ($p = 0.878$) to express GFP-Mn. The injection of AAV-GFP-Mn (AAV-GFP as control) in the amygdala (**f**) or hippocampus (**g**) did not change the density of Kv3.1b+ cells. In the images, GFP is in cyan, Kv3.1b in black and Hoechst in yellow. **h** High magnification confocal image of a PV+/Kv3.1b+ interneuron infected by AAV-GFP-Mn in the hippocampus. PV staining is in magenta. **i** Comparison of the Kv3.1b staining intensity between GFP- ($n = 35$) and GFP+ ($n = 26$) cells (Unpaired t-test, $p = 0.514$). **j** Kv3.1b signal intensity did not correlate with that of GFP ($R^2 = 0.008$). **k** High magnification confocal image of Kv3.1b intensity in axons with ($n = 47$) or without GFP-Mn ($n = 48$). **l** Comparison of the Kv3.1b staining intensity between GFP- and GFP+ axons. ($p = 0.001$). **j** Kv3.1b signal intensity was inversely correlated with that of GFP in axons ($R^2 = 0.388$). Scale bars, 300 μm in (**f**) and (**g**), and 30 μm in (**h**) and (**k**). Unpaired t-test: *, $p < 0.05$; **, $p < 0.01$; ***, $p < 0.001$.

a Hyperexcitability of CA3 pyramidal neurons caused by MAP6 deletion



b Increased activity of BLA neurons caused by MAP6 deletion



Supplementary Fig. S6: Hypothetic models of MAP6-mediated impact on the neural circuit in the hippocampus and amygdala.

a In the hippocampus, MAP6 deletion reduces fast spiking in PV+ GABAergic interneurons via reducing Kv3.1 channels, which in part leads to hyperexcitability of CA3 pyramidal neurons and hence memory

deficit, as well as hyperactivity. **b** In the amygdala, MAP6 deletion reduces fast spiking in PV+ GABAergic interneurons via reducing Kv3.1 channels in BLA (basolateral amygdala), which leads to increased activity of BLA projection neurons to CeA (the central amygdala) and hence risk avoidance reduction.